Journal Pre-proof

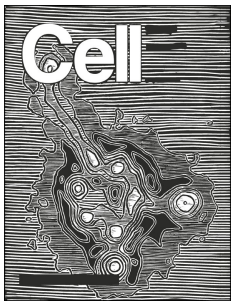

Loss of Bcl-6-expressing T follicular helper cells and germinal centers in COVID-19

Naoki Kaneko, Hsiao-Hsuan Kuo, Julie Boucau, Jocelyn R. Farmer, Hugues Allard-Chamard, Vinay S. Mahajan, Alicja Piechocka-Trocha, Kristina Lefteri, Matthew Osborn, Julia Bals, Yannic C. Bartsch, Nathalie Bonheur, Timothy M. Caradonna, Josh Chevalier, Fatema Chowdhury, Thomas J. Diefenbach, Kevin Einkauf, Jon Fallon, Jared Feldman, Kelsey K. Finn, Pilar Garcia-Broncano, Ciputra Adijaya Hartana, Blake M. Hauser, Chenyang Jiang, Paulina Kaplonek, Marshall Karpell, Eric C. Koscher, Xiaodong Lian, Hang Liu, Jinqing Liu, Ngoc L. Ly, Ashlin R. Michell, Yelizaveta Rassadkina, Kyra Seiger, Libera Sessa, Sally Shin, Nishant Singh, Weiwei Sun, Xiaoming Sun, Hannah J. Ticheli, Michael T. Waring, Alex L. Zhu, Galit Alter, Jonathan Z. Li, Daniel Lingwood, Aaron G. Schmidt, Matthias Lichterfeld, Bruce D. Walker, Xu Yu, Robert F. Padera, Jr., Shiv Pillai, and the Massachusetts Consortium on Pathogen Readiness Specimen Working Group

PII: S0092-8674(20)31067-9

DOI: https://doi.org/10.1016/j.cell.2020.08.025

Reference: CELL 11572

To appear in: *Cell*

Received Date: 2 July 2020

Revised Date: 24 July 2020

Accepted Date: 14 August 2020

Please cite this article as: Kaneko, N., Kuo, H.-H., Boucau, J., Farmer, J.R., Allard-Chamard, H., Mahajan, V.S., Piechocka-Trocha, A., Lefteri, K., Osborn, M., Bals, J., Bartsch, Y.C., Bonheur, N., Caradonna, T.M., Chevalier, J., Chowdhury, F., Diefenbach, T.J., Einkauf, K., Fallon, J., Feldman, J., Finn, K.K., Garcia-Broncano, P., Hartana, C.A., Hauser, B.M., Jiang, C., Kaplonek, P., Karpell, M., Koscher, E.C., Lian, X., Liu, H., Liu, J., Ly, N.L., Michell, A.R., Rassadkina, Y., Seiger, K., Sessa, L., Shin, S., Singh, N., Sun, W., Sun, X., Ticheli, H.J., Waring, M.T., Zhu, A.L., Alter, G., Li, J.Z., Lingwood, D., Schmidt, A.G., Lichterfeld, M., Walker, B.D., Yu, X., Padera Jr., R.F., Pillai, S., and the Massachusetts Consortium on Pathogen Readiness Specimen Working Group, Loss of Bcl-6-expressing T follicular helper cells and germinal centers in COVID-19, *Cell* (2020), doi: https://doi.org/10.1016/j.cell.2020.08.025.

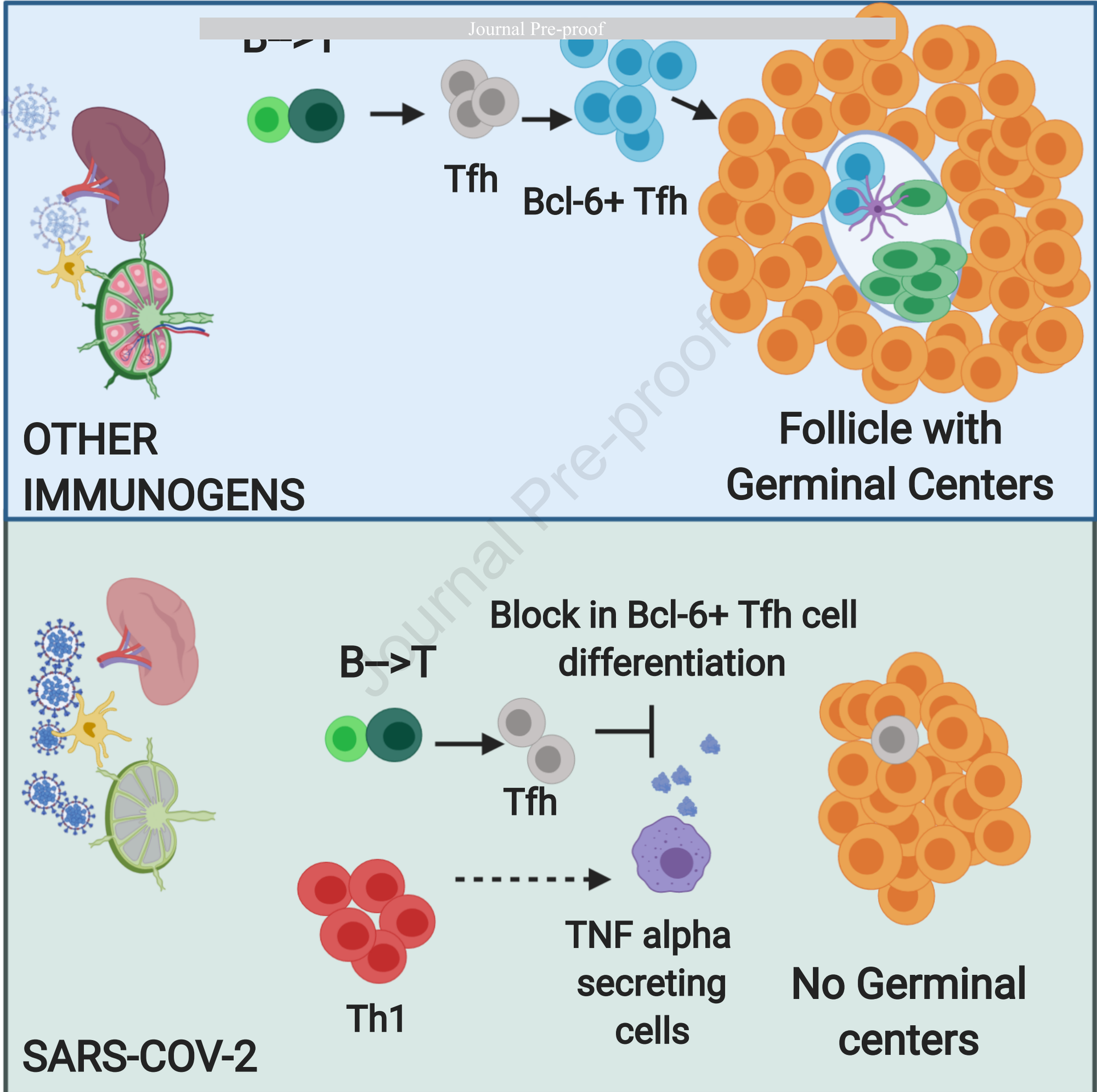

Loss of Bcl-6-expressing T follicular helper cells and germinal centers in COVID-19

Naoki Kaneko[1,8], Hsiao-Hsuan Kuo[1,8], Julie Boucau[1,8] , Jocelyn R. Farmer[1,8], Hugues Allard-Chamard[1,4], Vinay S. Mahajan[1,2], Alicja Piechocka-Trocha[1,6], Kristina Lefteri[1], Matthew Osborn[1], Julia Bals[1], Yannic C. Bartsch[1], Nathalie Bonheur[1], Timothy M. Caradonna[1], Josh Chevalier[1], Fatema Chowdhury[1], Thomas J. Diefenbach[1], Kevin Einkauf[1], Jon Fallon[1], Jared Feldman[1], Kelsey K. Finn[1], Pilar Garcia-Broncano[1], Ciputra Adijaya Hartana[1], Blake M. Hauser[1], Chenyang Jiang[1], Paulina Kaplonek[1], Marshall Karpell[1], Eric C. Koscher[1], Xiaodong Lian[1], Hang Liu[1], Jinqing Liu[1], Ngoc L. Ly[1], Ashlin R. Michell[1], Yelizaveta Rassadkina[1], Kyra Seiger[1], Libera Sessa[1], Sally Shin[1], Nishant Singh[1], Weiwei Sun[1], Xiaoming Sun[1], Hannah J. Ticheli[1], Michael T. Waring[1,6], Alex L. Zhu[1], Galit Alter[1], Jonathan Z. Li[3], Daniel Lingwood[1], Aaron G. Schmidt[1,5], Matthias Lichterfeld[1,3], Bruce D. Walker[1,6,7], Xu Yu[1], Robert F. Padera, Jr.[2,*], Shiv Pillai[1,9,*]and the Massachusetts Consortium on Pathogen Readiness Specimen Working Group

[1] Ragon Institute of MGH, MIT and Harvard, Cambridge, MA 02139, USA
[2] Department of Pathology, Brigham and Women's Hospital, Boston, MA 02115, USA
[3] Department of Medicine, Brigham and Women's Hospital, Boston, MA 02115, USA
[4] Division of Rheumatology, Faculté de médecine et des sciences de la santé de l'Université de Sherbrooke et Centre de Recherche Clinique Étienne-Le Bel, Sherbrooke, Québec, J1K 2R1, Canada
[5] Department of Microbiology, Harvard Medical School, Boston, MA 02115, USA
[6] Howard Hughes Medical Institute, Chevy Chase, MD 20815, USA
[7] Department of Biology and Institute of Medical Engineering and Science, Massachusetts Institute of Technology, Cambridge, MA 02139, USA
[8] These authors contributed equally
[9] Lead contact

[*] Correspondence: pillai@helix.mgh.harvard.edu (S.P.) and rpadera@bwh.harvard.edu (R.F.P.)

Summary

Humoral responses in COVID-19 disease are often of limited durability, as seen with other human coronavirus epidemics. To address the underlying etiology, we examined postmortem thoracic lymph nodes and spleens in acute SARS-CoV-2 infection and observed the absence of germinal centers, a striking reduction in Bcl-6^+ germinal center B cells but preservation of AID^+ B cells. Absence of germinal centers correlated with an early specific block in Bcl-6^+ T_{FH} cell differentiation together with an increase in T-bet^+ T_{H1} cells and aberrant extra-follicular TNF-α accumulation. Parallel peripheral blood studies revealed loss of transitional and follicular B cells in severe disease and accumulation of SARS-CoV-2-specific "disease-related" B cell populations. These data identify defective Bcl-6^+ T_{FH} cell generation and dysregulated humoral immune induction early in COVID-19 disease, providing a mechanistic explanation for the limited durability of antibody responses in coronavirus infections and suggest that achieving herd immunity through natural infection may be difficult.

Introduction

Adaptive immunity is initiated in secondary lymphoid organs and is influenced by the milieu generated by the initial activation of the innate immune system. Longitudinal studies on humoral immunity in COVID-19 as well as studies in convalescent subjects indicate that humoral immunity is often short lived and that most SARS-CoV-2 antibodies exhibit limited somatic hypermutation (Brouwer et al., 2020; Long et al., 2020; Robbiani et al., 2020). Understanding how the adaptive immune system is modulated in severe COVID-19 disease thus requires interrogation of secondary lymphoid organs in the acute phase of infection, where these responses are generated, but most studies to date have largely focused on peripheral blood samples.

SARS-CoV-2 infection results in a broad spectrum of clinical manifestations from asymptomatic to rapidly fatal, but the reasons for this heterogeneity are not known. Severely ill patients experience a life-threatening acute respiratory distress syndrome, and, even in an advanced care setting, some patients sustain severe lung damage and succumb early (Zhu et al. 2020; Zhou et al., 2020). Virus is found in the lungs and airways early in infection but not as the disease progresses (Schaefer et al., 2020). Damage-associated molecular patterns (DAMPs) released by infected pneumocytes likely combine with viral pathogen-associated molecular patterns (PAMPs) to activate innate immunity (Vardhana and Wolchok, 2020). The cytokine milieu thus generated would be predicted to influence the induction of lymphocyte activation by antigen conveyed directly in the lymph or by dendritic cells to draining lymph nodes. Viremia likely also leads to the initiation of immune responses in the spleen.

Many of the features of severe human coronavirus disease in COVID-19 and in SARS are strikingly similar. Progressive lymphopenia has been described in SARS-CoV-2 infection (Guan

et al., 2020) and the degree of lymphopenia has been correlated with increases in circulating IL-6 and IL-8 (Zhang et al., 2020). Lymphopenia was also observed in SARS at the peak of active disease which was also characterized by cytokine storm and acute respiratory distress (Perlman and Dandekar, 2005). Autopsy studies in SARS showed atrophy of lymphoid organs including lymph nodes, spleen and Peyer's patches and loss of germinal centers (Gu et al., 2005). Autopsy studies in COVID-19 have also identified splenic white pulp atrophy (Xu et al. 2020, Buja et al., 2020) and lymphocyte depletion in spleen and lymph nodes (Lax et al., 2020). However, numerous viral and non-viral infections do give rise to cytokine storm, acute respiratory distress and lymphopenia (Tisoncik et al., 2012). Splenic white pulp atrophy has also been histo-pathologically demonstrated in Ebola and Marburg disease (Martines et al., 2016; Rippey et. al., 1984) and in H5N1 influenza (Gao et al. 2010; Lu et al., 2008). These data, taken together, suggest that many different viral and infectious triggers can contribute to a similar constellation of immunological phenomena that may drive pathology.

In persons with COVID-19, the magnitude and durability of antibody responses are greater in those with more severe disease (Ju et al., 2020; Amanat et al., 2020) but are often of low magnitude (Robbiani et al., 2020) and appear to lack durability (Long et al., 2020). This may be similar to SARS and MERS where humoral responses were generally not durable except in a subset of individuals (Mo et al., 2006; Zumla et al., 2015). Impaired infection-induced protective immunity has also been documented by repeated infections with the human coronaviruses CoV 229E, NL63, OC43 and HKU1 in patients with less severe respiratory tract infections (Galanti et al., 2018). Reinfection could be possibly attributed to viral strain subtypes, but the reason/s for the general lack of durable humoral immune responses to coronaviruses has never been established.

A better understanding of alterations to components of the humoral immune system, especially in secondary lymphoid organs, provides an opportunity to decipher why natural infections with coronaviruses often do not provide durable immunity. A granular analysis of B and T lymphocytes in draining lymph nodes and spleens of SARS or MERS patients was never reported, leaving the underlying basis for the lymphopenia and the general lack of durability of antibody responses in those diseases unresolved. Since COVID-19 disease most significantly affects the lungs, we undertook an analysis of thoracic lymph nodes examining lymphoid architecture and lymphocyte populations using multi-color immunofluorescence, multispectral imaging and cell-cell interaction analyses from the time of disease onset in persons with diverse disease outcomes. Given that viremia has been observed in this illness (Zheng et al., 2020; Lescure et al., 2020) we also interrogated spleens both in the acute and late disease settings and complemented these studies with examination of peripheral blood samples in a separate cohort wherein convalescence could also be studied. Our results identify a striking absence of lymph node and splenic germinal centers and Bcl-6 expressing B cells, defective Bcl-6^+ T follicular helper cell generation and differentiation and dysregulated SARS-CoV-2 specific humoral immunity early in COVID-19 disease, providing a mechanistic explanation for the limited durability of humoral immunity and the less robust somatic hypermutation seen in this disease following natural infection.

Results

Absence of germinal centers, loss of Bcl-6$^+$ germinal center B cells but preservation of AID$^+$ B cells in lymph nodes early in COVID-19 disease

We have used a human tissue imaging platform with quantitative high-resolution automated slide-scanning microscopy, exploiting both regular and confocal approaches and multispectral imaging, in order to interrogate human lymphoid and non-lymphoid organs at the single cell level. These approaches crucially preserve architecture over broad swaths of tissue. Thoracic lymph nodes in severely ill COVID-19 patients who succumbed in less than eight days after admission (the group designated "Early"; less than 10 days from the onset of respiratory symptoms; **Table S1**), displayed a lack of germinal centers and these were also absent in those who succumbed later (15-36 days after admission, categorized as "Late") (**Fig. 1A, B**). Controls were thoracic lymph nodes from age matched individuals who succumbed from non-COVID-19 causes (**Table S2**). Quantitation revealed dramatic early loss of both B and T cells, absolute numbers declining to about a third of their non-COVID-19 controls, and this persisted in late disease (**Fig.1 D, E**), though distinct T and B cell zones could always be clearly discerned. Human control lymph nodes contain germinal centers possibly because of ongoing adaptive immunity initiated by commensal antigens. The absence of germinal centers in the thoracic lymph nodes of acutely ill COVID-19 patients in whose lungs we have already described very high viral loads (Schaefer et al., 2020) was particularly surprising.

Bcl-6 expressing germinal center B cells were also markedly reduced in COVID-19 but there was a preservation of AID expressing B cells, although these were diffusely distributed compared to controls (**Fig. 1C, F, G**).

Marked reduction in Bcl-6+ germinal center B cells in COVID-19 spleens

Analysis of spleens in this same group of COVID-19 patients also revealed a preponderance of red pulp and paucity of white pulp (**Fig. 2A, B**), a marked reduction in B and T cell numbers (**Fig. 2B, D, E**) and a marked reduction in Bcl-6^+ germinal center B cells (**Fig. 2C, F**). There was, however, very clear and quantitative preservation of AID^+ B cells in both early and late splenic tissue (**Fig. 2C, G**). Importantly follicular dendritic cells (FDC) were present in both lymph nodes and spleen in these patients, indicating that the lack of these cells was not contributing to the lack of germinal center B cells (**Fig. S1**). Together these data indicate that early in severe COVID-19 disease, even within ten days of the onset of respiratory symptoms, there is severe attrition in B and T cell numbers and a striking reduction in Bcl-6^+ B cells in lymph nodes and the spleen and the loss of germinal centers. Interestingly AID^+ B cells are preserved indicating that activated helper T cells are still likely to be in frequent contact with antigen specific B cells.

COVID-19-related reduction in $CD4^+CXCR5^+$Bcl-6^+ germinal center T follicular helper cells

To better understand the absence of germinal centers in COVID-19, we explored the possibility that the tissue milieu might contribute to defective T follicular helper cell differentiation. In both the lymph nodes and spleen, in early as well as late disease, $CD4^+$ $ICOS^+$ T_{FH} cells were diminished (**Fig. 3A, C, E, G**), and $CD4^+$ $CXCR5^+$ T_{FH} cells were present but reduced in numbers (**Fig. S2**) but the decrease in $CD4^+$ Bcl-6^+ germinal center type T_{FH} (GC-T_{FH}) cells was striking (**Fig. 3B, D, F and H).** Tissue quantitation confirmed significant differences for both early and late disease compared to controls**.** Because these changes were

seen both in thoracic lymph nodes and in the spleen these data are consistent with the view that circulating factors in severely ill COVID-19 patients may impair GC- T_{FH} cell differentiation and thus abrogate the generation of germinal centers. Although in principle phenotypically defined $CD4^+$ Bcl-6^+ T cells could include both T_{FH} cells and T follicular regulatory cells, we stained cells simultaneously with CD4, CXCR5, FOXP3 and Bcl-6 among other markers and used multispectral imaging to establish that while there were $FOXP3^+$ T regs present, there was no overlap in Bcl-6 and FoxP3 expression in COVID-19 secondary lymphoid organs, indicating that there are very few if any T follicular regulatory cells in COVID-19 (**Fig. S3A**). Although there is a developmental role for TNF-α in primary lymphoid follicular development (Pasparakis et al., 1996; Korner et al., 1997), germinal center loss has been described in the context of cytokine storm in mouse models, has been reversed by TNF-α blockade (Ryg-Cornejo et al., 2016, Popescu et al., 2019) and also linked genetically to an abundance of TNF-α (Popescu et al., 2019). We therefore also examined activated secondary lymphoid tissues from controls and COVID-19 lymph nodes for TNF-α expression. In this case we used tonsils from non-COVID infected patients as a control for activated lymphoid tissue. While TNF-α is expressed at low levels in the follicle in controls, in COVID-19 it is expressed very abundantly both inside and outside the follicle (**Fig. S3C and D**). These data indicate that the differentiation of activated $CD4^+$ T cells into GC-type Bcl-6^+ T_{FH} cells is specifically blocked in COVID-19. Given the information obtained from the above animal models (Popescu et al., 2019; Ryg-Cornejo et al., 2016), it is possible that the aberrant and exuberant synthesis of TNF-α at the site of T_{FH} differentiation in COVID-19 lymph nodes may contribute to the lack of germinal centers and the impaired quality and durability of the antibody response to SARS-CoV-2 in this disease.

Increased frequency of secondary lymphoid organ T_{H1} cells in severe COVID-19

We hypothesized that the reduction in GC-T_{FH} cell numbers likely reflects a block in differentiation, and next sought to determine if this reduction was specific to this particular $CD4^+$ T cell subset. We quantitated $CD4^+$ T cell subsets in the lymph nodes and spleens using the well-established transcription factors T-bet, GATA-3, RORγt and FOXP3 as key markers. In contrast to the reduced GC-T_{FH} cell numbers, T_{H1} cells were consistently increased early and late in both the lymph nodes and spleen, whereas an increase in T_{H17} cells was more variable (**Fig. 4**). In contrast, a consistent reduction in T_{H2} cells was observed (**Fig. 4**). Late in the disease $FOXP3^+$ Tregs made up a large part of the population of $CD4^+$ T cells. Overall there was an increase in secondary lymphoid organ $CD4^+$ T cells relative to $CD8^+$ T cells in COVID-19 secondary lymphoid organs though this was variable (**Fig. S4**). These data indicate that the defect in GC-type T_{FH} cell differentiation is specific and suggest that this defect may be indirectly linked to the strong T_{H1} response seen in this disease.

Follicular and extra-follicular T-B conjugates and activated IgD^-CD27^- double negative B cells in COVID19 lymph nodes and spleens

The preservation in COVID-19 of AID^+ B cells and the relatively large proportions of $CD4^+$ $CXCR5^+$ T_{FH} cells (that do not express Bcl-6) and T_{H1} cells, both known to express CD40L, led us to hypothesize that even though there were no germinal centers, there may be frequent T-B conjugates in COVID-19 within follicles as well as in extra-follicular locations. The absence of germinal centers (most germinal center B cells are $IgD^-CD27^-Bcl\text{-}6^+AID^+CXCR5^+$ $CD19^+$ cells) offered the opportunity to directly ask whether many of the

scattered activated AID^+ B cells inside and outside follicles in COVID-19 secondary lymphoid organs were also IgD^-CD27^- "double negative" B cells. These cells are often observed in chronic infectious contexts including in viral infections as well as in autoimmunity (Portugal et al., 2017; Jenks et al., 2019). They are considered to be "disease-related" cells and are generally described as "extra-follicular", implying they are not derived from the germinal center reaction, but are frequently class switched and have the hallmarks of having been induced in a T-dependent manner without germinal center based selection. At extra-follicular and follicular sites these double negative B cells may be less capable of inducing the differentiation of the Bcl-6^+GC-T_{FH} cells that are required to induce germinal centers.

By applying computational tools to systematically quantitate the area of cytoplasmic overlap between sets of two cells of two different cell types, and using pre-determined cut-offs to assess true cell-cell interaction, we quantified the degree and intimacy of plasma membrane contacts between cells and observed the presence of numerous T-B conjugates in COVID-19 lymph nodes and spleens (**Fig. S5**). The presence of IgD^-CD27^- double negative cells both within and outside follicles in COVID-19 lymph nodes and spleens was clearly evident (**Fig. S5**). IgG expressing class-switched plasmablasts were prominent both within the follicular and extra-follicular areas (**Fig. S3B**). These data indicate that in the absence of germinal center formation in COVID-19 an "extra-follicular" type of class-switched B cell response, more typical of disease rather than of long-lasting protection, predominates in secondary lymphoid organs.

Decreases in early transitional and follicular B cells in severe COVID-19 patients correlate with systemic inflammation

While the interrogation of secondary lymphoid organs from autopsies helps provide snapshots regarding the sites of the induction of the immune response, we sought to obtain information from patients at different stages of the disease, including convalescence and ongoing severe illness, by the use of extended flow cytometry panels by examining peripheral blood from patients. Given the observed accumulation of activated non-germinal center derived B cells such as $IgD^{-}CD27^{-}$ double negative B cells in COVID-19 lymphoid organs, we examined whether similar activated B cell populations with binding specificity for SARS-CoV-2 could be found in the circulation in persons with disparate disease severity.

Patients were divided into gradations of severity that included asymptomatic convalescence and active severe illness requiring hospitalization that was further subdivided by intermediate (CRP < 200 mg/L; 'CRP int') and high (CRP > 200 mg/L; 'CRP hi') levels of maximum inflammatory marker elevation (**Table S4**). Studies on freshly isolated PBMCs revealed that the proportions and absolute numbers of total $CD19^{+}$ B cells in addition to naïve ($IgD^{+}CD27^{-}$), early transitional T1 and T2 ($IgD^{+}CD27^{-}CD10^{+}CD45RB^{-}$), and $CXCR5^{+}$ follicular ($IgD^{+}CD27^{-}CD10^{-}CD73^{+}$; Farmer et al., 2019) B cell subsets were markedly reduced in severely ill COVID-19 patients with high CRP levels as compared to convalescent patients and healthy controls (**Fig. 5A, B, S6, S7**). The relative loss of these naïve B cells correlated with the maximum level of CRP elevation (**Fig. 5C**) and with the clinical parameters of symptom duration at the time of blood draw and total days of hospital admission for loss of early transitional B cells, specifically (**Fig. 5D**). These data suggest a direct association between these B cell phenotypic changes in blood and patient clinical morbidity from COVID-19. They indicate that in the milieu of severe COVID-19, B cells either develop very inefficiently in the

bone marrow or are possibly generated but acquire an activated phenotype and are lost. This results in a marked reduction in early transitional and follicular B cells and likely further compounds defects in humoral immunity.

Increased proportions of activated naïve B cells, IgD$^-$CD27$^-$CXCR5$^-$ B cells and plasmablasts in severely ill COVID-19 patients correlate with systemic inflammation and are specific for SARS-CoV-2

Within the CD27$^+$ memory B cell compartment, total switched memory (IgD$^-$) B cells, including activated (CD21^{lo}) switched memory B cells and plasmablasts were significantly elevated (as a proportion of all B cells) in severely ill COVID-19 patients with high CRP levels as compared to convalescent COVID-19 patients and healthy controls (**Fig. 6A, B**), though in terms of absolute numbers these relative increases were blunted by the greater degree of B cell lymphopenia (**Fig. S7**). Within the IgD$^+$CD27$^-$ compartment, severely ill patients with COVID-19 and high CRP levels, specifically, showed an increase in a number of disease-related presumed non-germinal center derived activated B cells as compared to convalescent patients. These include activated naïve B cells (IgD$^+$CD27$^-$CD21^{lo}CD11c^{hi}) (Kaminski et al., 2012) as well as atypical late transitional B cells (IgD$^+$CD27$^-$CD10$^-$CD73$^-$CXCR5$^-$) (**Fig. 6C**). Additionally, IgD$^-$CD27$^-$CXCR5$^-$ B cells that include populations described by Kaminski et al. based on the expression of CXCR5 and CD11c were expanded in severely ill COVID-19 patients with high CRP levels, specifically, as compared to convalescent patients and healthy controls

(**Fig. 6D**). The sum accumulation of these activated B cells was markedly higher in the severely ill COVID-19 patients with high versus intermediate CRP levels and also in comparison to convalescent patients and healthy controls (**Fig. 6E**). Paralleling the trends observed with the loss of early transitional B cells, the gain in circulating activated B cells correlated with higher CRP levels and increased patient morbidity as measured by symptom duration and length of inpatient hospitalization (**Fig. 6F**).

Although recent studies have also documented circulating activated B cell populations in COVID-19 patients (Mathew et al.,2020; Kuri-Cervantes et al., 2020; Woodruff et al., 2020) the antigen specificity of these cells was not evaluated. We tested whether the activated B cell populations we had identified were specific for the SARS-CoV-2 Spike receptor binding domain (RBD) using recombinant RBD labeled separately with APC and PE fluorophores. Cells that stained with both labeled probes were considered authentic RBD-specific B cells (**Fig. 7A**). This probe contains a very small fraction of all the potential antibody epitopes in SARS-CoV-2 but is highly specific for this particular virus (Premkumar et al., 2020). All the activated and mainly disease-related populations of relevance in COVID-19 contain SARS-CoV-2 specific cells (**Fig. 7A, B**), establishing that they were expanded as a result of an adaptive immune response to this virus. In particular the presence of antigen-specific double negative B cells, switched memory B cells, and plasmablasts are all consistent with an extra-germinal center/extra-follicular type class-switched antibody response to SARS-CoV-2. These data establish that the aberrant non-germinal center type activated B cells that accumulate in tissues also accumulate in the blood of severely ill and convalescent COVID-19 patients and these include virus-specific B cells. Given that they bear the hallmarks of not being from germinal centers, they are therefore unlikely to provide optimal or durable humoral immunity.

Discussion

Long-lasting B cell memory and the highest affinity pathogen-specific antibodies are derived within germinal centers in secondary lymphoid organs. Germinal centers are anatomically structured to facilitate the selection of high affinity B cell with long life spans (Victora and Nussenzweig, 2012). Longevity of such responses exceeds decades for some infectious diseases and when a substantial portion of a population is infected, can contribute to herd immunity. In contrast, antibody responses to SARS-CoV-2 appear to be similar to other human coronaviruses in being short-lived in a large fraction of individuals (Long et al., 2020). Understanding the reasons for this decline in responses requires architectural studies of lymphoid organs from patients coupled with cell-cell interaction analyses, as well as approaches to reliably identify, quantify and physically locate the diverse immune cell types that contribute to antibody induction. Using quantitative multicolor immunofluorescence combined with multispectral imaging and cell-cell interaction analyses of autopsy specimens as well as analyses of peripheral blood samples in parallel cohorts with acute SARS-CoV-2 infection, we show evidence for dysregulated humoral immune induction early in COVID-19 including a striking absence of germinal centers in the earliest stages of infection, defective $Bcl6^+$ T_{FH} cell generation and aberrant lymphoid TNF-α production.

The absence of Bcl-6^+ T follicular helper cells (and the consequent absence of germinal centers) in COVID-19 secondary lymphoid organs provides an explanation for a phenomenon anecdotally observed in autopsies of many different severe viral infections. These findings also provide a mechanistic basis for the recent descriptions of non-durable humoral immune responses, impaired humoral immunity and the low levels of somatic hypermutation in antibodies from convalescent COVID-19 patients (Long et al., 2020; Robbiani et al., 2020;

Brouwer et al., 2020). The alteration of the cytokine milieu in secondary lymphoid organs in this disease likely reflects a continuum across the spectrum of disease. While T-dependent B cell activation, class switching and some low level somatic hypermutation do occur in COVID-19, the germinal center reaction is sub-optimal or totally absent and this will likely, in due course of time, be reflected in less durable class-switched antibody responses similar to those seen in SARS and MERS. These findings have some bearing on concepts such as herd immunity and immunity passports following natural infection with SARS-CoV-2. They strongly underscore the need and relevance of vaccination approaches to the prevention of COVID-19.

Severe infections by many different human viruses result in high levels of circulating cytokines and peripheral lymphopenia, but few studies have examined secondary lymphoid organs where immune responses are generated. Autopsy studies have revealed lymphoid depletion of the spleen and lymph nodes in Ebola, Marburg, and in H5N1 (Martines et al., 2015; Rippey et al., 1984; Lu et al., 2008; Gao et al., 2010). In SARS, lymphoid depletion and loss of germinal centers was also reported (Gu et al., 2005). Autopsy studies in these severe viral infections had not systematically examined lymphoid populations in secondary lymphoid organs. More detailed mechanistic studies of tissues have been undertaken in murine model systems. In a mouse model of severe malaria, germinal center responses were defective, and this was linked to a defect in T follicular helper cell differentiation (Ryg-Cornejo et al., 2016) that could be reversed by TNF-α blockade. *Ehrlichia muris* infection in mice has also been associated with the loss of germinal centers and TNF-α blockade restored germinal centers as did the genetic deletion of TNF-α (Popescu et al, 2019). A mouse immunization model that involved prior generation of specific $CD4^+$ T cell memory prior to infection with lymphocytic choriomeningitis virus generated a severe cytokine storm, splenic shrinkage, loss of germinal centers and bone

marrow hypocellularity suggesting that lymphopenia and lymphoid organ abnormalities may be attributed to immune mechanisms rather than being a direct consequence of viral cytolysis (Penaloza-Macmaster, 2015). These studies in mice, taken together, suggest that significant elevation of secreted cytokines and chemokines seen in the context of protozoan, bacterial and viral infections can cause the loss of germinal centers.

The studies of Ryg-Cornejo et al. in murine malaria and our studies in COVID-19 suggest that the observed cytokine and chemokine dysregulation may block germinal center type T follicular helper cell differentiation. The contribution of TNF-α to follicular development and germinal center formation (Pasparakis et al.,1996; Korner et al.,1997) as well as to the loss of germinal centers is complex and seemingly contradictory (Ryg-Cornejo et al., 2016; Popescu et al., 2019). Local cytokine concentrations at the site of T follicular helper cell differentiation likely have important consequences for the germinal center reaction. The differentiation of $CD4^+Bcl\text{-}6^-CXCR5^+$ pre-germinal center T_{FH} cells into $CD4^+Bcl\text{-}6^+CXCR5^+$ GC- T_{FH} cells likely occurs extra-follicularly at the T-B interface (Kerfoot et al., 2011; Kitano et al., 2011; Crotty S, 2014; Vinuesa et al., 2016). Based on our findings, we suspect that the very high local levels of TNF-α and possibly other cytokines at this location in COVID-19 lymph nodes, possibly induced downstream of T_{H1} cell activation, block the final step in T follicular helper cell differentiation. In the murine malaria model IFN-γ blockade also restored T_{FH} cells and germinal centers, consistent with T_{H1} cells being upstream of the induction of TNF-α. Given that $Bcl\text{-}6^+$ B cells, $Bcl\text{-}6^+$ T_{FH} cells and $Bcl\text{-}6^+$ T follicular regulatory cells are all extremely sparse or absent in COVID-19 secondary lymphoid organs, the formal possibility that excessive TNF signaling (or excessive signaling by some combination of cytokines in the extra-follicular area) negatively

impacts the expression of *BCL6* either transcriptionally or post-transcriptionally also needs to be investigated. Such deeper mechanistic studies can best be pursued in murine models.

Because of our focus on the loss of germinal centers, we have concentrated on TNF-α because of its known ability, when produced in excess, to contribute to impaired T_{FH} cell differentiation and germinal center loss. Many other cytokines are induced in COVID-19 and probably contribute to some aspects of the phenotypes that we describe here. IL-6, for example, though it has pleiotropic effects, is known to suppress lymphopoiesis and induce myelopoiesis (Maeda et al., 2009), and it might thus contribute to the B lymphopenia that we document here.

Altered extra-follicular B cell activation could potentially also contribute to a defect in T follicular helper cell differentiation observed in SARS-CoV-2 infection. After the initial activation of naive $CD4^+$ T cells by dendritic cells presenting the relevant MHC class II molecule and peptide, along with co-stimulation, these T cells activate antigen-specific B cells that present the same MHC-peptide complex and extra-follicular B cell foci are generated. It is in this vicinity that pre-germinal center T follicular helper cells are first generated, and we have shown in humans (Maehara et al., 2018) as others have in mice (Roco et al., 2019) that most isotype switching actually occurs at this location. In COVID -19 it is likely that some antibody generation occurs extra-follicularly, though we have identified IgG expressing plasmablasts extra-follicularly as well as in the follicles bereft of germinal centers. Activated B cells expressing ICOSL provide additional differentiation signals to activated $CD4^+$ T cells to acquire high levels of CXCR5, induce the expression of Bcl-6 and migrate into the follicles as fully differentiated germinal center type T follicular helper cells, that set up the germinal center reaction. Perhaps because cytokine alterations lead to the formation of dysfunctional B cells and

plasmablasts outside the follicle, activated B cells in COVID-19 may be less capable of inducing cognate T cells to differentiate into germinal center type T follicular helper cells.

It is possible that our investigations may throw some light on the mechanisms of disease progression in severe COVID-19, although a deeper understanding will likely await the acquisition of more knowledge and the development of suitable animal models. The evasion of the anti-viral aspects of innate immunity and the overly aggressive activation of inflammation by the virus likely results in an altered milieu that contributes both to the relative attenuation of $CD8^+$ T cell immunity and prevents the generation of Bcl-6^+ T follicular helper cells. As a result of the latter, the early development of high affinity antibodies that could contribute to some attenuation of viral spread may be compromised. Whether the increased $CD4^+/CD8^+$ T cell ratio we observe in lymph nodes and spleens of COVID-19 patients reflects selective activation of $CD4^+$ T cells or a preferential depletion of $CD8^+$ T cells is unclear. Why certain individuals are more prone to initial more aggressive and destructive immune responses also remains a very difficult question to address at this time. Based on our analyses, severe disease does not appear to be due to a paucity of regulatory T cells in secondary lymphoid organs at the earlier stages of the disease, though our approaches do not interrogate Treg function. The striking relative accumulation of $FoxP3^+$ regulatory T cells that we observe late in disease could possibly reflect a homeostatic mechanism for the resolution of infection. More likely it reflects the reduced overall numbers of recirculating T cells entering lymphoid organs and the recurring activation of naive $CD4^+$ T cells into activated subsets that egress these lymphoid organs while lymphoid organ-resident regulatory T cells perhaps do not leave these sites and therefore appear to accumulate in lymph nodes and the spleen.

In summary, even in acutely ill COVID-19 patients, at a time when they have extremely high viral loads and abundant virus has been demonstrated in their lungs, there is a striking absence of germinal centers associated with a marked reduction of germinal center B cells, but preservation of AID-expressing B cells. Thus, though there is robust T cell mediated activation of B cells, germinal centers do not form. The robust activation of non-germinal center type B cell responses does not give rise to long-lived memory or high affinity B cells. The underlying basis for the loss of germinal centers is best explained by the striking failure of differentiation of Bcl-6^+ T follicular helper cells likely because of dramatic changes in the extra-follicular cytokine milieu driven by T_{H1} cells and the aberrant local production of TNF-α in lymphoid organs. We believe these findings will be relevant to a range of human viral and non-viral diseases in which there is a cytokine storm, a better understanding of which will require a granular function-focused analysis of the architecture and composition of lymph nodes and spleens. We predict that a broadly applicable common mechanistic basis similar to what we describe here will be elucidated in future studies on MERS, H1N1, Ebola, Marburg and other viral diseases.

Limitations of the Study: Our studies on secondary lymphoid organs focused by necessity on very ill patients, and while changes in the disease may represent a continuum, it is quite possible that patients with less severe disease may induce better germinal center responses. Of necessity the numbers for thoracic lymph node and spleen were relatively small. We used a single approach to study lymphocyte populations in the lymph nodes and the spleen, and the complementary use of an orthogonal approach would have been ideal.

Consortia: *Mass CPR Specimen Working Group*: Betelihem A. Abayneh, Patrick Allen, Diane Antille, Katrina Armstrong, Alejandro Balazs, Max Barbash, Siobhan Boyce, Joan Braley, Karen Branch, Katherine Broderick, George Daley, Ashley Ellman, Liz Fedirko, Keith Flaherty, Jeanne Flannery, Pamela Forde, Elise Gettings, David Golan, Amanda Griffin, Sheila Grimmel, Kathleen Grinke, Kathryn Hall, Meg Healey, Howard Heller, Deborah Henault, Grace Holland, Chantal Kayitesi, Evan C Lam, Vlasta LaValle, Yuting Lu, Sara Luthern, Jordan Marchewska, Brittni Martino, Ilan Millstrom, Noah Miranda, Christian, Nambu, Susan Nelson, Marjorie Noone, Claire O'Callaghan, Christine Ommerborn, Lois Chris Pacheco, Nicole Phan, Falisha A. Porto, Alexandra Reissis, Francis Ruzicka, Edward Ryan, Katheleen Selleck, Arlene Sharpe, Christianne Sharr, Sue Slaugenhaupt, Kimberly Smith Sheppard, Elizabeth Suschana, Vivine Wilson, Daniel Worrall

Acknowledgments: We thank Doug Kwon and Brooke Spencer of the Ragon Institute for access to Ragon Institute Tissue core specimens and Andrew Lichtman of BWH Pathology for helpful advice. This work was supported by NIH U19 AI110495 to SP, NIH R01 AI146779 to AGS, NIH R01AI137057 and DP2DA042422 to DL, BMH was supported by NIGMS T32 GM007753, TMC was supported by T32 AI007245. Funding for these studies from the Massachusetts Consortium of Pathogen Readiness, the Mark and Lisa Schwartz Foundation and Enid Schwartz is also acknowledged. The graphical abstract was prepared using Biorender.

Author Contributions: Conceptualization (SP, RJP, NK, JRF, HK, JBo, BDW, XY); Methodology (HA-C, NK, JRF, TD, MW, HK, JBo); Investigation (NK, HK, JBo, AP-T, KL, MO, JBa, YB, NB, JC, FC, KE, JFa, KKF, PG-B,CH, CJ, PK, MK, XL, HL, JL, NL, ARM, YR,

KS, JS, SS, NS, WS, XS, HJT, ALZ, RFP); Resources (RFP, BDW, XY, JL, VSM, DL, AGS, BMH, JFe, TMC, JBa, GA, ML); Original Draft (SP, NK, JRF, JBo, HK); Review/Editing (SP, BDW, NK, JRF, HK, JBo, HAC); Supervision (SP, XY)

Declaration of Interests: SP is on the SAB of Abpro Inc. and Pulsar Biopharma. GA is founder of Seromyx Systems Inc.

Legends to Figures

Figure 1. Early loss of germinal centers and Bcl-6 expressing B cells in COVID-19 thoracic lymph nodes

(A) Hematoxylin–eosin staining of lymph nodes from early (left) and late (right) COVID-19 patients. (B) Low-power images of CD3 (red), CD19 (green), Bcl-6 (orange) and DAPI (blue) staining in a lymph node from a late COVID-19 patient (left) and a non-COVID-19 thoracic lymph node (right). (C) Representative multi-color immunofluorescence images of CD3 (red), CD19 (green), Bcl-6 (orange) and AID (purple) staining in lymph nodes from early (left) and late (middle) COVID-19 patients and a non-COVID-19 lymph node (right). (D and E) Absolute numbers of $CD19^+$ B cells (D) and $CD3^+$ T cells (E) in lymph nodes from COVID-19 patients (purple, n = 11) and non-COVID-19 patients (blue, n = 6). COVID-19 samples include early (purple, n = 5) and late (red, n = 6) COVID-19 patients. (F and G) Absolute numbers and relative proportion of $Bcl6^+$ B cells (F) and AID^+ B cells (G) in the pool of $CD19^+$ B cells in lymph nodes from COVID-19 patients (purple, n = 11) and non-COVID-19 patients (blue, n = 6). COV-19 = COVID-19, LN= Lymph node. Mann-Whitney U test used to calculate p-value. Error bars represent mean ±SEM. **p < 0.01; ***p < 0.001. See Also Fig. S1 and Tables S1 and S2.

Figure 2. White pulp attrition, early loss of germinal centers and Bcl-6 expressing B cells in COVID-19 spleens

(A) Cross-sectional view of whole spleen and hematoxylin–eosin staining from early (left) and late (right) COVID-19 patients. (B) Low-power images of CD3 (red), CD19 (green), Bcl-6 (orange) and DAPI (blue) staining in a spleen from a late COVID-19 patient (left) and a control

(right). (C) Representative multi-color immunofluorescence image of CD3 (red), CD19 (green), Bcl-6 (orange) and AID (purple) staining in spleens from a late COVID-19 patient (left) and a control (right). (D and E) Absolute numbers of $CD19^+$ B cells (D) and $CD3^+$ T cells (E) in spleens from early (purple, n = 4) and late (red, n = 6) COVID-19 patients and controls (blue, n = 7). (F and G) Absolute numbers and relative proportion of Bcl-6^+ B cells (F) and AID^+ B cells (G) in spleens from early (purple, n = 4) and late (red, n = 6) COVID-19 patients and controls (blue, n = 7). SP=Spleen. Multiple comparisons are controlled for by Kruskal-Wallis test. Error bars represent mean ±SEM. *$p < 0.05$. See also Tables S2 and S3.

Figure 3. Loss of germinal center type Bcl6+ T follicular helper cells in COVID-19 lymph nodes and spleens

(A) Representative multi-color immunofluorescence image of CD4 (red), ICOS (green) and DAPI (blue) staining in lymph nodes from early (left) and late (middle) COVID-19 patients and a non-COVID-19 control (right). Arrows indicate $CD4^+$ $ICOS^+$ T_{FH} cells. (B) Representative multi-color immunofluorescence images of CD4 (red), Bcl6 (white) and DAPI (blue) staining in lymph nodes from early (left) and late (middle) COVID-19 patients and a non-COVID-19 control (right). Arrows indicate $CD4^+$ $Bcl6^+$ GC-type T_{FH} cells. (C) Representative multi-color immunofluorescence images of CD4 (red), ICOS (green) and DAPI (blue) staining in spleens from early (left) and late (middle) COVID-19 patients and a control (right). (D) Representative multi-color immunofluorescence images of CD4 (red), Bcl6 (white) and DAPI (blue) staining in spleens from early (left) and late (middle) COVID-19 patients and a control (right). (E and F) Absolute numbers and relative proportions of $CD4^+$ $ICOS^+$ T_{FH} cells (E) and $CD4^+$ $Bcl6^+$ GC-type T_{FH} cells (F) in lymph nodes from COVID-19 patients (purple, n = 11) and non-COVID-19

patients (blue, n = 6). COVID-19 samples include early (purple, n = 5) and late (red, n = 6) COVID-19 patients. (G and H) Relative proportions of $CD4^+$ $ICOS^+$ T_{FH} cells (G) and $CD4^+$ $Bcl6^+$ GC-type T_{FH} (H) in spleens from COVID-19 patients (purple, n = 10) and controls (blue, n = 7). COVID-19 samples include early (purple, n = 4) and late (red, n = 6) COVID-19 patients. Mann-Whitney U test used to calculate p-value. Error bars represent mean ±SEM. *p < 0.05; **p < 0.01; ***p < 0.001. See also Fig. S2, S3 and S4 and Tables S1, S2 and S3.

Figure 4. T_{H1} cells are expanded in comparison to other CD4+T cell subsets in COVID-19 thoracic lymph nodes and spleens

(A) Representative multi-color staining showing T_{H1}, T_{H2}, T_{H17} and Treg cells in lymph nodes form early (left) and late (middle) COVID-19 patients and a non-COVID-19 control (right). [T_{H1}: $CD4^+$ (red) T-bet^+ (light blue)] [T_{H2}: $CD4^+$ (red) $GATA3^+$ (purple)] [T_{H17}: $CD4^+$ (red) $ROR\gamma^+$ (yellow)] [Treg: $CD4^+$ (red) $FoxP3^+$ (green)]. (B) Absolute numbers and relative proportions of T_{H1}, T_{H2}, T_{H17} and Treg cells in lymph nodes and spleens (purple) from early (purple, lymph nodes: n = 5, spleens: n = 4) and late (red, n = 6) COVID-19 patients and controls (blue, lymph nodes: n = 6, spleens: n = 7). Mann-Whitney U test used to calculate p-value. Error bars represent mean ±SEM. *p < 0.05; **p < 0.01. See also Figs. S5, S6 and S7 and Tables S1, S2 and S3.

Figure. 5. Decreased early transitional and follicular B cells in the peripheral blood of patients with severe COVID-19

Quantitation of (**A**) total $CD19^+$ B cells and (**B**) naïve, early transitional (T1/2), and follicular (FO) B cell subsets in the peripheral blood of patients with COVID-19 at states of convalescence

(n=39), severe illness with an intermediate maximum CRP level during hospitalization (< 200 mg/L; severe (CRP int); n=10), and severe illness with a high maximum CRP level during hospitalization (> 200 mg/L; severe (CRP hi); n=15) as defined by the clinical criteria listed in **Table S4** and compared to healthy controls (n=4). Quantitation shown by B cell level for each individual patient with mean, standard deviation, and significance by one-way ANOVA of log % B cell value indicated (*P < 0.05, **P < 0.01, ***P < 0.001, ****P < 0.0001). Representative COVID-19 contour plots shown (**B**) with healthy control contour plots and full B cell flow cytometry gating strategy outlined (**Fig. S6)**. Association of peripheral blood B cell frequency with maximum CRP level (**C**) and the clinical parameters of symptom duration at blood draw and total length of hospital stay (**D**) in all symptomatic COVID-19 patients (n=29) with moderate to severe illness as defined by the clinical criteria listed in **Table S4**. Correlation show by linear regression with individual patients, 95% confidence bands, R^2 and P values shown. See also Figs. S6 and S7 and Table S4.

Figure. 6. Increased proportions of activated B cell subsets in the peripheral blood of patients with severe COVID-19

Proportions of (**A**) switched memory (SM) B cells, (**B**) plasmablasts, (**C**) activated naïve and CXCR5- late transitional (T3a) B cells, (**D**) IgD^-CD27^- double negative (DN) B cells, and (**E**) total (sum) activated B cells in the peripheral blood of patients with COVID-19 at states of convalescence (n=39), severe illness with an intermediate maximum CRP level during hospitalization (< 200 mg/L; severe (CRP int); n=10), and severe illness with a high maximum CRP level during hospitalization (> 200 mg/L; severe (CRP hi); n=15) as defined by the clinical criteria listed in **Table S4** and compared to healthy controls (n=4). Quantitation shown by B cell

level for each individual patient with mean, standard deviation, and significance by one-way ANOVA of log % B cell value indicated (*P < 0.05, **P < 0.01, ***P < 0.001, ****P < 0.0001). Representative COVID-19 contour plots shown with healthy control contour plots and full B cell flow cytometry gating strategy outlined (**Fig. S6)**. (**F**) Association of activated B cell frequency in peripheral blood with maximum CRP level, symptom duration at blood draw, and total length of hospital stay in all symptomatic COVID-19 patients (n=29) with moderate to severe illness as defined by the clinical criteria listed in **Table S4**. Correlation show by linear regression with individual patients, 95% confidence bands, R^2 and P values shown. See also Figs. S6 and S7 and Table S4.

Figure. 7. Activated B cell subsets in the peripheral blood of patients with COVID-19 are specific for SARS-CoV-2-RBD

(A) Representative dot plots showing positive SARS-CoV-2-RBD staining in total $CD19^+$ B cells (left; boxed in red) and B cell subsets (right; colored in red). (**B**) All $CD19^+$ B cells binding to SARS-CoV-2-RBD shown for COVID-19 patients at states of convalescence (n=10) and severe illness (n=4) with summation of total % CoV-2-RBD reactivity by indicated B cell subset and quantitated as mean +/- SD with significance by Student's t-test of log % B cell value indicated (*p < 0.05). DN2 and DN3 Double negative B cells are CXCR5 low, while DN1 and DN4 B cells are CXCR5 high. Antibody-secreting (Ab-secreting), double negative (DN), marginal zone precursor (MZP), switched memory (SM), transitional (T), unswitched memory (USM). Ab-secreting cells included both plasmablasts and plasma cell, though the latter were very rare. See also Figs. S6 and Table S4.

Supplemental Figure Legends

Figure S1. FDCs are not lost in COVID-19 lymph nodes. Related to Figure 1. Representative multi-color immunofluorescence images of CD19 (red), Bcl6 (white), CD35 (green) and DAPI (blue) staining in lymph nodes from late COVID-19 patient (lower panel) and controls (upper panels).

Figure S2. Decrease in CXCR5$^+$ T follicular helper cells in COVID-19 lymph nodes and spleens. Related to Figure 3.

(A) Representative multi-color immunofluorescence images of CD4 (red), CXCR5 (green) and DAPI (blue) staining in lymph nodes from early (left) and late (middle) COVID-19 patients and a non-COVID-19 lymph node (right). Arrows indicate CD4$^+$ CXCR$^+$ T_{FH} cells. (B) Representative multi-color immunofluorescence images of CD4 (red), CXCR5 (green) and DAPI (blue) staining in spleens from early (left) and late (middle) COVID-19 patients and a control (right). (C and D) Absolute numbers (C) and relative proportions (D) of CD4$^+$ CXCR5$^+$ T_{FH} cells in lymph nodes and spleens from COVID-19 patients and non-COVID-19 lymph nodes (blue) (n = 6) and control spleens (blue) (n = 7). COVID-19 samples include early (purple; lymph node; n = 5) (spleen; n = 4) and late (red dots) (n = 6) COVID-19 patients. Mann-Whitney U test used to calculate p-value. Error bars represent mean ±SEM. **p < 0.01; ***p < 0.001.

Figure S3. (A) Increased T regs but no differentiation into TFR cells in COVID-19 lymph nodes. Related to Figure 3. Representative multi-spectral 7 color immunofluorescence images showing CD4 (red), CD19 (green), CXCR5 (purple), Bcl6 (white) FoxP3 (yellow), IgG (light

blue) and DAPI (blue) staining of lymph nodes from late COVID-19 patients. Images in the green box show high-power images. No $FoxP3^+/Bcl6^+$ cells were seen (white staining with no yellow overlap) in follicles.

(B) IgG^+ plasmablasts are found in follicular and extrafollicular areas in COVID-19 lymph nodes. Related to Figure 3. Representative multi-color immunofluorescence images of Bcl6 (white) and IgG (light blue) in lymph nodes of a late COVID-19 patient (left) and a control (right). IgG^+ cells were abundant in follicular and extrafollicular areas in both COVID-19 lymph nodes and controls.

(C and D) Large increase in TNF-α production at both follicular and extra-follicular sites in COVID-19 lymph nodes, while controls have low levels of TNF-α localized to follicles. Related to Figure 3.

(C**)** Representative multi-color immunofluorescence images of TNF-α (green) and DAPI (blue) staining in lymph nodes from early and late COVID-19 patients and a control. (D) Absolute numbers (left) and percentages (right) of TNF-α+ cells in lymph nodes from early (purple) (n = 5) and late (red; n = 6) COVID-19 patients and controls (blue; n = 10). Multiple comparisons were controlled for by Kruskal-Wallis test. Error bars represent mean ±SEM. *p < 0.05; **p < 0.01.

Figure S4. Increase in $CD4^+/CD8^+$ T cell ratio in lymph nodes and spleens in COVID-19. Related to Figure 4. (A) Representative multi-color immunofluorescence images of CD4 (red), CD8 (green) and DAPI (blue) staining in lymph nodes (top 2 rows of images) and spleens (bottom 2 rows of pictures) from early (left) and late (middle) COVID-19 patients and controls (right). (B) Relative ratios of CD4 and CD8 T cells (No./mm^2) in lymph nodes (left) and spleens

(right) from early (purple) (n=5/4) and late (red) (n=6) COVID-19 patients and controls (blue) (n=10/7).

Figure S5. Follicular and extra-follicular T-B conjugates and IgD$^-$CD27$^-$ B cells in COVID-19 lymph nodes. Related to Figure 4. (A) Immunofluorescence staining of CD3 (red), CD19 (green) and DAPI (blue) in a lymph node (top) and a spleen (bottom) in a late COVID-19 patient. Arrows and arrowheads indicate CD3$^+$ T cells and CD19$^+$ B cells respectively. T cell and B cells formed close and extensive intercellular plasma membrane contacts as highlighted in the yellow box. (B) Immunofluorescence staining (left panels) and visualization of T-B conjugates (middle and right panels) in a lymph node from a late COVID-19 patient using the Strata Quest cell-to-cell contact application. Masks of the nuclei based on DAPI staining establish the inner boundary of the cytoplasm and the software "looks" outwards towards the plasma membrane boundary. An overlap of at least 3 pixels of adjacent cell markers was required to establish each "contact" criterion. Details are in the Methods section. Nuclei circled in red and green respectively depict CD3$^+$ T cells and CD19$^+$ B cells in T-B conjugates. Each box (purple, light blue and yellow) highlights a T-B conjugate. (C) Representative multi-color immunofluorescence image of CD19 (red), IgD and CD27 (both in green) and DAPI (blue) staining in a lymph node from an early COVID-19 patient. IgD$^-$/CD27$^-$ double negative B cells (red staining with no green overlap) are abundant inside the follicle and also outside. Boxed area depicts some of these cells outside the follicle. White arrows show IgD$^-$/CD27$^-$ double negative B cells.

Figure S6. Analysis of circulating B cell subsets by flow cytometry. Related to Figures 5-7.

(A) Gating strategy for COVID-19 PBMCs. (B) Representative flow plots of relevant B cell subsets from PBMCs derived from a healthy donor. Antibody-secreting (Ab-secreting), double negative (DN), follicular (FO), marginal zone precursor (MZP), switched memory (SM), transitional (T), unswitched memory (USM).

Figure S7. Quantitation of B cells. Related to Figures 5 and 6. Quantitation of absolute B cell counts was undertaken in all COVID-19 patients in whom a proximal absolute lymphocyte count (ALC) was available in the electronic medical record at states of convalescence (n=5), severe illness with an intermediate maximum CRP level during hospitalization (< 200 mg/L; severe (CRP int); n=10), and severe illness with a high maximum CRP level during hospitalization (> 200 mg/L; severe (CRP hi); n=15) as defined by the clinical criteria listed in **Table S4**. Data are compared to healthy controls (n=4), assuming a healthy control ALC of 2.9 (K/uL). Quantitation shown by B cell level for each individual patient with mean, standard deviation, and significance by one-way ANOVA of log % B cell value indicated (*P < 0.05, **P < 0.01, ***P < 0.001) for (A) total $CD19^+$ B cells, (B) naïve, early transitional (T1/2), and follicular (FO) B cell subsets, (C) activated and double negative (DN) B cell subsets as indicated, and (D) activated and DN B cell subsets as a ratio to the available precursor population (naïve, IgD^+CD27^-).

STAR* Methods

KEY RESOURCES TABLE

REAGENT	SOURCE	IDENTIFIER
Antibodies		
Anti-CD3	BD Biosciences	Clone UCHT1
Anti-CD56	BD Biosciences	Clone NCAM16.2
Anti-CD19	BioLegend	Clone SJ25C1
Anti-CD27	BD Biosciences	Clone L128
Anti-IgD	BioLegend	Clone IA6-2
Anti-CD38	BioLegend	Clone HB-7
Anti-CD10	BioLegend	Clone HI10a
Anti-CD45RB	BioLegend	Clone MEM-55
Anti-CD21	BD Biosciences	Clone B-ly4
Anti-CD73	BioLegend	Clone AD2
Anti-CD138	BioLegend	Clone MI15
Anti-CD11c	BioLegend	Clone Bu15
Anti-CXCR5	BioLegend	Clone J252D4
Anti-CD20	BioLegend	Clone 2H7
Anti CD3	DAKO	Clone A045229-2
Anti-CD4	Biocare Medical	Clone CM153A
Anti-CD19	Biocare Medical	Clone SKU310
Anti-Bcl-6	Biocare Medical	Clone LN22
Anti-AID	Invitrogen	Clone ZA001
Anti-T-bet	Abcam	Clone ab150440
Anti-GATA-3	Biocare Medical	Clone CM405A
Anti-ICOS	Cell Signaling Technology	Clone 89601
Anti-Rorc	Abcam	Clone ab212496
Anti-CXCR5	R&D Systems	Clone MAB190
Anti-FOXP3	Cell Signaling Technology	Clone 98377
Ant-CD8	Abcam	Clone ab85972
Anti-IgD	DAKO	Clone AA093
Anti-CD27	Abcam	Clone ab131254
Anti-IgG	Abcam	Clone ab109489
Anti-TNF-α	Abcam	Clone ab6671
Anti-CD35	Abcam	Clone ab25
Chemicals and Recombinant Proteins		
Prolong Diamond Antifade Mountant with DAPI	Invitrogen	CAT#P36962
Opal Manual Multiplex IHC Kit	Perkin Elmer	CAT#NEK811001KT
FcR Blocking Reagent	Miltenyi Biotec	CAT#130-059-901
Rainbow Calibration Particles	ThermoFisher	CAT#A34305
LIVE/DEAD Fixable Blue Dead Cell Stain Kit	ThermoFisher	CAT# L23105

4% Paraformaldehyde solution	Santa Cruz Biotechnology	CAT#sc-281692
Streptavidin-APC conjugate	Life Technologies	CAT#S32362
Streptavidin-PE conjugate	Life Technologies	CAT#S21388
Freestyle Expression Medium	Thermo Scientific	CAT#123388018
Dulbecco's Phosphate buffer saline	Corning	CAT#21031
Fetal Bovine Serum (HyClone)	Fisher Scientific	CAT#SH3007003
TALON Metal Affinity Resin	Takara	CAT#635652

Experimental Models: Cell Lines

Human Expi293F	Thermo Fisher	CAT#A14527

Recombinant DNA

pVRC-SARS-CoV-2-RBD	This study	N/A

Software and Algorithms

FlowJo	FlowJo	www.flowjo.com
FACSDIVA	BD Biosciences	www.bdbiosciences.com/en-us/instruments/research-instruments/research-software/flow-cytometry-acquisition/facsdiva-software
Prism 8	GraphPad Software	www.graphpad.com/scientific-software/prism/
TissueQuest	TissueGnostics	www.tissuegnostics.com/products/software/tissuequest
StrataQuest	TissueGnostics	www.tissuegnostics.com/products/software/strataquest

RESOURCE AVAILABILITY

Lead Contact

Further information and requests for resources and reagents should be directed to and will be fulfilled by the Lead Contact, Dr. Shiv Pillai pillai@helix.mgh.harvard.edu

Materials Availability

The SARS-CoV-2 RBD protein is made freely available through Dr. Aaron Schmidt who may be reached through the Lead Contact or directly.

Data and Code Availability

The published article includes all data generated or analyzed during this study, and summarized in the accompanying tables, figures and Supplemental materials.

EXPERIMENTAL MODEL AND SUBJECT DETAILS

Human Subjects

Tissue analysis Cohort

Thoracic lymph nodes and spleens samples from COVID-19 patients were obtained through the Brigham and Women's hospital Department of Pathology.

Sample Size Estimation: Power calculations and sample size estimation were not performed before the initiation of this study which was based primarily on the availability of COVID-19 positive autopsies for analysis between March and May 2020. All cases were retrieved from the Anatomic Pathology files of Brigham and Women's Hospital and included 17 patients (information on age and gender in Table S1and S2) including 11 with laboratory confirmed COVID-19 who underwent autopsy in 2020.

Sample allocation to experimental groups: All patients had tested positive for SARS-CoV-2 by RT-PCR of nasopharyngeal swabs in a laboratory during hospital admission. All cases were divided into two groups; early (less than ten days from respiratory symptoms onsets to death, hospitalization of up to 8 days), and late (hospitalized for 15-36 days prior to death). Thoracic lymph nodes were obtained from six age-matched non-COVID-19 patients who underwent autopsies at the Brigham and Women's Hospital in the same time window. In addition, seven spleens from automobile accident victims were obtained from the Ragon Institute Tissue Core. These were histologically normal. Information on age and gender is in Table S3. Ten discarded control tonsils from Massachusetts General Hospital not matched for age and gender were also used for initial titration and validation of certain antibodies and as controls for TNF-α and CD8 staining studies,

Peripheral Blood Cohort

Peripheral blood samples were drawn from both Outpatients and Inpatients with COVID-19 at Massachusetts General Hospital and fresh blood was analyzed for flow cytometry using a multi-color panel.

Sample Size estimation: Power calculations were not undertaken pior to the initiation of these studies. However, the primary end-point was the sum of activated B cells (as a % CD19+ B cells in peripheral blood). Using a two sided Student's t-test to compare log values of convalescent and severe (CRP hi) COVID-19 patient samples, with groups of 10, we had more than 90% power to detect an effect of size of 1.20 between groups based on simulation studies using 10,000 Monte Carlo samples with a type 1 error rate of 5%.

Allocation to Experimental Groups: Data is presented on B cell populations from 68 patients, including moderately ill, severely ill and convalescent patients. Convalescence was defined as a clinically asymptomatic state on the date of blood draw, either from a baseline asymptomatic state or recuperated from moderate clinical symptoms of COVID- 19. Moderate disease was defined as active clinical symptoms of COVID-19 on the date of blood draw that did not necessitate a hospital admission. Severe disease was defined as active clinical symptoms of COVID-19 on the date of blood draw that did necessitate a hospital admission. Severe disease was further subdivided by maximum CRP level during hospital admission as CRP < 200 mg/L classified as ‘CRP intermediate (int)’ and CRP > 200 mg/L as ‘CRP high (hi).’

Study Approval

This study was performed with the approval of the Institutional Review Boards at the Massachusetts General Hospital and the Brigham and Women's Hospital.

METHOD DETAILS

Multi-color immunofluorescence staining

Tissue samples were fixed in formalin, embedded in paraffin, and sectioned. These specimens were incubated with the following antibodies: anti-CD3 (clone: A045229-2; DAKO), anti-CD4 (clone: CM153A; Biocare Medical), anti-CD19 (clone: SKU310; Biocare Medical), anti-Bcl6 (clone: LN22; Biocare Medical), anti-AID (clone: ZA001; Invitrogen), anti-T-bet (clone: ab150440; Abcam), GATA3 (clone: CM405A; Biocare), ICOS (clone: 89601; Cell Signaling Technology), Rorc (clone: ab212496; Abcam), CXCR5 (clone: MAB190; R&D Systems), Foxp3 (clone: 98377; Cell Signaling Technology), anti-CD8 (clone: ab85792; Abcam), anti-IgD (clone: AA093; DAKO), anti-CD27 (clone: ab131254; Abcam), anti-IgG (clone: ab109489; Abcam), anti-TNF-α (clone: ab6671; Abcam), and anti-CD35 (clone: ab25; Abcam) followed by incubation with a secondary antibody using an Opal™ Multiplex Kit (Perkin Elmer). The samples were mounted with ProLong™ Diamond Antifade mountant containing DAPI (Invitrogen).

Microscopy and Quantitative Image Analysis

Images of the tissue specimens were acquired using the TissueFAXS platform (TissueGnostics). For quantitative analysis, the entire area of the tissue was acquired as a digital grayscale image in five channels with filter settings for FITC, Cy3, Cy5 and AF75 in addition to DAPI. Cells of a given phenotype were identified and quantitated using the TissueQuest software

(TissueGnostics), with cut-off values determined relative to the positive controls. This microscopy-based multicolor tissue cytometry software permits multicolor analysis of single cells within tissue sections similar to flow cytometry. In addition, multispectral images (seven-colors staining) were unmixed using spectral libraries built from images of single stained tissues for each reagent using the StrataQuest (TissueGnostics) software. StrataQuest software was also used to quantify cell-to-cell contact. In the StrataQuest cell-to-cell contact application, masks of the nuclei based on DAPI staining establish the inner boundary of the cytoplasm and the software "looks" outwards towards the plasma membrane boundary. Overlap of at least 3 pixels of adjacent cell markers is required to establish a "contact" criterion. Although the software has been developed and validated more recently, the principle of the method and the algorithms used have been described in detail elsewhere (Ecker et al., 2004).

Flow cytometry

1 Million fresh PBMCs were stained within 2 hours of isolation. Prior to antibody staining, Fc receptors were blocked using human FcR blocking reagent (Miltenyi) at a concentration of 1:50 at 4 ℃ for 10 minutes. Cells were surface stained at 4 ℃, protected from light, using optimized concentrations of fluorochrome-conjugated primary antibodies for 30 minutes as well as live/dead fixable blue stain (Thermo Fisher) at a concentration of 1:20 using the following antibody panels (clone, manufacturer).

B cell panel: CD3 (UCHT1, BD Biosciences), CD56 (NCAM16.2, BD Biosciences) CD19 (SJ25C1, BioLegend), CD27 (L128, BD Biosciences), IgD (IA6-2, BD Biosciences), CD38 (HB-7, BioLegend), CD10 (HI10a, BioLegend), CD21 (B-ly4, BD Biosciences), CD73 (AD2,

BioLegend), CD45RB (MEM-55, BioLegend), CD138 (MI15, BioLegend), CD11c (Bu15, BioLegend), and CXCR5 (J252D4, BioLegend; RF8B2 BD Bioscience).

For the RBD-specific characterization, 6-7 million fresh PBMCs were stained using fluorescently labeled SARS-CoV-2 RBD in addition to the B cell panel antibodies listed above.

Cells were then washed in PBS and fixed using 4% paraformaldehyde for 30 minutes at at 4 □. Flow cytometry was performed on a BD Symphony (BD Biosciences, San Jose, CA) and rainbow tracking beads (8 peaks calibration beads, Fisher) were used to ensure consistent signals between flow cytometry batches. FCS files were analyzed, and B cell subsets were quantified using FlowJo software (version 10).

RBD Expression and Purification

SARS-2 RBD (GenBank: MN975262.1) was cloned into pVRC vector containing an HRV 3C-cleavable C-terminal SBP-His_{8X} tag and sequence confirmed by Genwiz. The construct was transiently transfected into mammalian Expi293F suspension cells for recombinant expression. 5 days post-transfection, supernatants were harvested and clarified by low-speed centrifugation. The RBD was purified by immobilized metal affinity chromatography (IMAC) using Cobalt-TALON resin (Takara) followed by size exclusion chromatography on Superdex 200 Increase 10/300 GL (GE Healthcare) in PBS. Purity was assessed by SDS-PAGE analysis. The fluorescent PE-SA (Invitrogen, Cat#12-4317-877) and APC-SA (Invitrogen; Cat#S32362) labels were added to the purified SBP-tagged RBD proteins through iterative complex formation, as previously described (Weaver et al. 2016). The fluorescent SA conjugates were added to SBP-RBD in five increments to sequentially form the complexes. In this case the final molar ratio of probe to streptavidin valency was 1:1 (one SA-fluorophore can bind two SBP tags). After each

stepwise addition of the fluorescent label, the mixture was incubated for 20 minutes and set rotating at 4C within an opaque 1.5 mL Eppendorf spin tube. Using this method, we generated fluorescent probes at a final concentration of 0.1ug/ul. An example of SBP-RBD (31,000g/mol) labeled with PE-SA (300,000g/mol) is described for a total 10 assays (0.5 ug labeled protein per assay): First, 5uL of SBP-RBD at 1ug/ul was diluted in 20.8uL PBS. Fluorescent PE-SA at 1ug/ul was then added in five increments, with an incremental volume of 4.8 uL for a final volume of 50uL.

QUANTIFICATION AND STATISTICAL ANALYSIS

Flow cytometry, clinical correlations and tissue studies. GraphPad Prism version 8 was used for statistical analysis, curve fitting and linear regression. A two-tailed Mann-Whitney U test was used to calculate p-values for continuous, non-parametric variables. For comparing more than one population, Kruskal-Wallis testing was used with Dunn's multiple comparison testing. A p-value of < 0.05 was considered significant.

List of Supplementary Tables

REFERENCES

Amanat, F., Stadlbauer, D., Strohmeier, S., Nguyen, T.H.O., Chromikova, V., McMahon, M., Jiang, K., Arunkumar, G.A., Jurczyszak, D., Polanco, J.*, et al.* (2020). A serological assay to detect SARS-CoV-2 seroconversion in humans. Nat Med. 26, 1033-36.

Brouwer, P.J.M., Caniels, T.G., van der Straten, K., Snitselaar, J.L., Aldon, Y., Bangaru, S., Torres, J.L., Okba, N.M.A., Claireaux, M., Kerster, G.*, et al.* (2020). Potent neutralizing antibodies from COVID-19 patients define multiple targets of vulnerability. Science. 369, 643-650

Buja, L.M., Wolf, D.A., Zhao, B., Akkanti, B., McDonald, M., Lelenwa, L., Reilly, N., Ottaviani, G., Elghetany, M.T., Trujillo, D.O.*, et al.* (2020). The emerging spectrum of cardiopulmonary pathology of the coronavirus disease 2019 (COVID-19): Report of 3 autopsies from Houston, Texas, and review of autopsy findings from other United States cities. Cardiovasc Pathol *48*, 107233.

Cao, W.C., Liu, W., Zhang, P.H., Zhang, F., and Richardus, J.H. (2007). Disappearance of antibodies to SARS-associated coronavirus after recovery. N Engl J Med *357*, 1162-1163.
Crotty, S. (2014). T follicular helper cell differentiation, function, and roles in disease. Immunity *41*, 529-542.

Ecker, R.C., and Steiner, G.E. (2004). Microscopy-based multicolor tissue cytometry at the single-cell level. Cytometry A *59*, 182-190.

Farmer, J.R., Allard-Chamard, H., Sun, N., Ahmad, M., Bertocchi, A., Mahajan, V.S., Aicher, T., Arnold, J., Benson, M.D., Morningstar, J.*, et al.* (2019). Induction of metabolic quiescence defines the transitional to follicular B cell switch. Sci Signal *12*.eaaw 5573.

Galanti, M., Birger, R., Ud-Dean, M., Filip, I., Morita, H., Comito, D., Anthony, S., Freyer, G.A., Ibrahim, S., Lane, B.*, et al.* (2019). Longitudinal active sampling for respiratory viral infections across age groups. Influenza Other Respir Viruses *13*, 226-232.

Gao, R., Dong, L., Dong, J., Wen, L., Zhang, Y., Yu, H., Feng, Z., Chen, M., Tan, Y., Mo, Z.*, et al.* (2010). A systematic molecular pathology study of a laboratory confirmed H5N1 human case. PLoS One *5*, e13315.

Gu, J., Gong, E., Zhang, B., Zheng, J., Gao, Z., Zhong, Y., Zou, W., Zhan, J., Wang, S., Xie, Z.*, et al.* (2005). Multiple organ infection and the pathogenesis of SARS. J Exp Med *202*, 415-424.

Guan, W.J., Ni, Z.Y., Hu, Y., Liang, W.H., Ou, C.Q., He, J.X., Liu, L., Shan, H., Lei, C.L., Hui, D.S.C.*, et al.* (2020). Clinical Characteristics of Coronavirus Disease 2019 in China. N Engl J Med *382*, 1708-1720.

Jenks, S.A., Cashman, K.S., Woodruff, M.C., Lee, F.E., and Sanz, I. (2019). Extrafollicular responses in humans and SLE. Immunol Rev *288*, 136-148.

Ju, B., Zhang, Q., Ge, J., Wang, R., Sun, J., Ge, X., Yu, J., Shan, S., Zhou, B., Song, S.*, et al.* (2020). Human neutralizing antibodies elicited by SARS-CoV-2 infection. Nature.584, 115-119.

Kaminski, D.A., Wei, C., Rosenberg, A.F., Lee, F.E., and Sanz, I. (2012). Multiparameter flow cytometry and bioanalytics for B cell profiling in systemic lupus erythematosus. Methods Mol Biol *900*, 109-134.

Kerfoot, S.M., Yaari, G., Patel, J.R., Johnson, K.L., Gonzalez, D.G., Kleinstein, S.H., and Haberman, A.M. (2011). Germinal center B cell and T follicular helper cell development initiates in the interfollicular zone. Immunity *34*, 947-960.

Kitano, M., Moriyama, S., Ando, Y., Hikida, M., Mori, Y., Kurosaki, T., and Okada, T. (2011). Bcl6 protein expression shapes pre-germinal center B cell dynamics and follicular helper T cell heterogeneity. Immunity *34*, 961-972.

Korner, H., Cook, M., Riminton, D.S., Lemckert, F.A., Hoek, R.M., Ledermann, B., Kontgen, F., Fazekas de St Groth, B., and Sedgwick, J.D. (1997). Distinct roles for lymphotoxin-alpha and tumor necrosis factor in organogenesis and spatial organization of lymphoid tissue. Eur J Immunol *27*, 2600-2609.

Kuri-Cervantes, L., Pampena, M.B., Meng, W., Rosenfeld, A.M., Ittner, C.A.G., Weisman, A.R., Agyekum, R.S., Mathew, D., Baxter, A.E., Vella, L.A.*, et al.* (2020). Comprehensive mapping of immune perturbations associated with severe COVID-19. Sci Immunol *5*, eabd 7114

Lax, S.F., Skok, K., Zechner, P., Kessler, H.H., Kaufmann, N., Koelblinger, C., Vander, K., Bargfrieder, U., and Trauner, M. (2020). Pulmonary Arterial Thrombosis in COVID-19 With Fatal Outcome: Results from a Prospective, Single-Center, Clinicopathologic Case Series. Ann Intern Med.

Lescure, F.X., Bouadma, L., Nguyen, D., Parisey, M., Wicky, P.H., Behillil, S., Gaymard, A., Bouscambert-Duchamp, M., Donati, F., Le Hingrat, Q.*, et al.* (2020). Clinical and virological data of the first cases of COVID-19 in Europe: a case series. Lancet Infect Dis *20*, 697-706.

Long, Q.X., Liu, B.Z., Deng, H.J., Wu, G.C., Deng, K., Chen, Y.K., Liao, P., Qiu, J.F., Lin, Y., Cai, X.F.*, et al.* (2020). Antibody responses to SARS-CoV-2 in patients with COVID-19. Nat Med *26*, 845-848.

Lu, M., Xie, Z.G., Gao, Z.C., Wang, C., Li, N., Li, M., Shao, H.Q., Wang, Y.P., and Gao, Z.F. (2008). [Histopathologic study of avian influenza H5N1 infection in humans]. Zhonghua Bing Li Xue Za Zhi *37*, 145-149.

Maeda, K., Malykhin, A., Teague-Weber, B.N., Sun, X.H., Farris, A.D., and Coggeshall, K.M. (2009). Interleukin-6 aborts lymphopoiesis and elevates production of myeloid cells in systemic lupus erythematosus-prone B6.Sle1.Yaa animals. Blood *113*, 4534-4540.

Maehara, T., Mattoo, H., Mahajan, V.S., Murphy, S.J., Yuen, G.J., Ishiguro, N., Ohta, M., Moriyama, M., Saeki, T., Yamamoto, H.*, et al.* (2018). The expansion in lymphoid organs of IL-4(+) BATF(+) T follicular helper cells is linked to IgG4 class switching in vivo. Life Sci Alliance *1*.e201800050.

Martines, R.B., Ng, D.L., Greer, P.W., Rollin, P.E., and Zaki, S.R. (2015). Tissue and cellular tropism, pathology and pathogenesis of Ebola and Marburg viruses. J Pathol *235*, 153-174.

Mathew, D., Giles, J.R., Baxter, A.E., Oldridge, D.A., Greenplate, A.R., Wu, J.E., Alanio, C., Kuri-Cervantes, L., Pampena, M.B., D'Andrea, K.*, et al.* (2020). Deep immune profiling of COVID-19 patients reveals distinct immunotypes with therapeutic implications. Science.eabc 8511

Mo, H., Zeng, G., Ren, X., Li, H., Ke, C., Tan, Y., Cai, C., Lai, K., Chen, R., Chan-Yeung, M.*, et al.* (2006). Longitudinal profile of antibodies against SARS-coronavirus in SARS patients and their clinical significance. Respirology *11*, 49-53.

Pasparakis, M., Alexopoulou, L., Episkopou, V., and Kollias, G. (1996). Immune and inflammatory responses in TNF alpha-deficient mice: a critical requirement for TNF alpha in the formation of primary B cell follicles, follicular dendritic cell networks and germinal centers, and in the maturation of the humoral immune response. J Exp Med *184*, 1397-1411.

Penaloza-MacMaster, P., Barber, D.L., Wherry, E.J., Provine, N.M., Teigler, J.E., Parenteau, L., Blackmore, S., Borducchi, E.N., Larocca, R.A., Yates, K.B.*, et al.* (2015). Vaccine-elicited CD4 T cells induce immunopathology after chronic LCMV infection. Science *347*, 278-282.

Perlman, S., and Dandekar, A.A. (2005). Immunopathogenesis of coronavirus infections: implications for SARS. Nat Rev Immunol *5*, 917-927.

Popescu, M., Cabrera-Martinez, B., and Winslow, G.M. (2019). TNF-alpha Contributes to Lymphoid Tissue Disorganization and Germinal Center B Cell Suppression during Intracellular Bacterial Infection. J Immunol *203*, 2415-2424.

Portugal, S., Obeng-Adjei, N., Moir, S., Crompton, P.D., and Pierce, S.K. (2017). Atypical memory B cells in human chronic infectious diseases: An interim report. Cell Immunol *321*, 18-25.

Premkumar, L., Segovia-Chumbez, B., Jadi, R., Martinez, D.R., Raut, R., Markmann, A., Cornaby, C., Bartelt, L., Weiss, S., Park, Y.*, et al.* (2020). The receptor binding domain of the viral spike protein is an immunodominant and highly specific target of antibodies in SARS-CoV-2 patients. Sci Immunol *5*, eabc8413

Rippey, J.J., Schepers, N.J., and Gear, J.H. (1984). The pathology of Marburg virus disease. S Afr Med J *66*, 50-54.

Robbiani, D.F., Gaebler, C., Muecksch, F., Lorenzi, J.C.C., Wang, Z., Cho, A., Agudelo, M., Barnes, C.O., Gazumyan, A., Finkin, S.*, et al.* (2020). Convergent antibody responses to SARS-CoV-2 in convalescent individuals. Nature.

Roco, J.A., Mesin, L., Binder, S.C., Nefzger, C., Gonzalez-Figueroa, P., Canete, P.F., Ellyard, J., Shen, Q., Robert, P.A., Cappello, J.*, et al.* (2019). Class-Switch Recombination Occurs Infrequently in Germinal Centers. Immunity *51*, 337-350 e337.

Ryg-Cornejo, V., Ioannidis, L.J., Ly, A., Chiu, C.Y., Tellier, J., Hill, D.L., Preston, S.P., Pellegrini, M., Yu, D., Nutt, S.L.*, et al.* (2016). Severe Malaria Infections Impair Germinal Center Responses by Inhibiting T Follicular Helper Cell Differentiation. Cell Rep *14*, 68-81.

Schaefer, I.M., Padera, R.F., Solomon, I.H., Kanjilal, S., Hammer, M.M., Hornick, J.L., and Sholl, L.M. (2020). In situ detection of SARS-CoV-2 in lungs and airways of patients with COVID-19. Mod Pathol. 19, 1-11.

Teijaro, J.R., Njau, M.N., Verhoeven, D., Chandran, S., Nadler, S.G., Hasday, J., and Farber, D.L. (2009). Costimulation modulation uncouples protection from immunopathology in memory T cell responses to influenza virus. J Immunol *182*, 6834-6843.

Tisoncik, J.R., Korth, M.J., Simmons, C.P., Farrar, J., Martin, T.R., and Katze, M.G. (2012). Into the eye of the cytokine storm. Microbiol Mol Biol Rev *76*, 16-32.

Victora, G.D., and Nussenzweig, M.C. (2012). Germinal centers. Annu Rev Immunol *30*, 429-457.

Vinuesa, C.G., Linterman, M.A., Yu, D., and MacLennan, I.C. (2016). Follicular Helper T Cells. Annu Rev Immunol *34*, 335-368.

Weaver, G.C., Villar, R.F., Kanekiyo, M., Nabel, G.J., Mascola, J.R., and Lingwood, D. (2016). In vitro reconstitution of B cell receptor-antigen interactions to evaluate potential vaccine candidates. Nat Protoc *11*, 193-213.

Woodruff, M., Ramonell, R., Cashman, K., Nguyen, D., Ley, A., Kyu, S., Saini, A., Haddad, N., Chen, W., Howell, J.C.*, et al.* (2020). Critically ill SARS-CoV-2 patients display lupus-like hallmarks of extrafollicular B cell activation. medRxiv. 2020.04.29.20083717

Xu, X., Chang, X.N., Pan, H.X., Su, H., Huang, B., Yang, M., Luo, D.J., Weng, M.X., Ma, L., and Nie, X. (2020). [Pathological changes of the spleen in ten patients with new coronavirus infection by minimally invasive autopsies]. Zhonghua Bing Li Xue Za Zhi *49*, E014.

Zhang, X., Tan, Y., Ling, Y., Lu, G., Liu, F., Yi, Z., Jia, X., Wu, M., Shi, B., Xu, S.*, et al.* (2020). Viral and host factors related to the clinical outcome of COVID-19. Nature. 583, 437-440

Zheng, H.Y., Zhang, M., Yang, C.X., Zhang, N., Wang, X.C., Yang, X.P., Dong, X.Q., and Zheng, Y.T. (2020). Elevated exhaustion levels and reduced functional diversity of T cells in peripheral blood may predict severe progression in COVID-19 patients. Cell Mol Immunol *17*, 541-543.

Zheng, S., Fan, J., Yu, F., Feng, B., Lou, B., Zou, Q., Xie, G., Lin, S., Wang, R., Yang, X.*, et al.* (2020). Viral load dynamics and disease severity in patients infected with SARS-CoV-2 in Zhejiang province, China, January-March 2020: retrospective cohort study. BMJ *369*, m1443.

Zhou, P., Yang, X.L., Wang, X.G., Hu, B., Zhang, L., Zhang, W., Si, H.R., Zhu, Y., Li, B., Huang, C.L.*, et al.* (2020). A pneumonia outbreak associated with a new coronavirus of probable bat origin. Nature *579*, 270-273.

Zhu, N., Zhang, D., Wang, W., Li, X., Yang, B., Song, J., Zhao, X., Huang, B., Shi, W., Lu, R.*, et al.* (2020). A Novel Coronavirus from Patients with Pneumonia in China, 2019. N Engl J Med *382*, 727-733.

Zumla, A., Hui, D.S., and Perlman, S. (2015). Middle East respiratory syndrome. Lancet *386*, 995-1007.

Highlights

1. Acute phase SARS-CoV-2-specific T cells display an activated cytotoxic phenotype
2. Broad and polyfunctional SARS-CoV-2-specific T cell responses in convalescent phase
3. Detection of SARS-CoV-2-specific T cell responses also in seronegative individuals

eTOC Blurb

Buggert and colleagues provide a phenotypic and functional map of SARS-CoV-2-specific T cells across the full spectrum of exposure, infection, and COVID-19 severity. They observe that SARS-CoV-2-specific T cells generate a broad, robust and functionally replete response in convalescent individuals, that may provide protection from recurrent episodes of severe COVID-19.

Figure 1

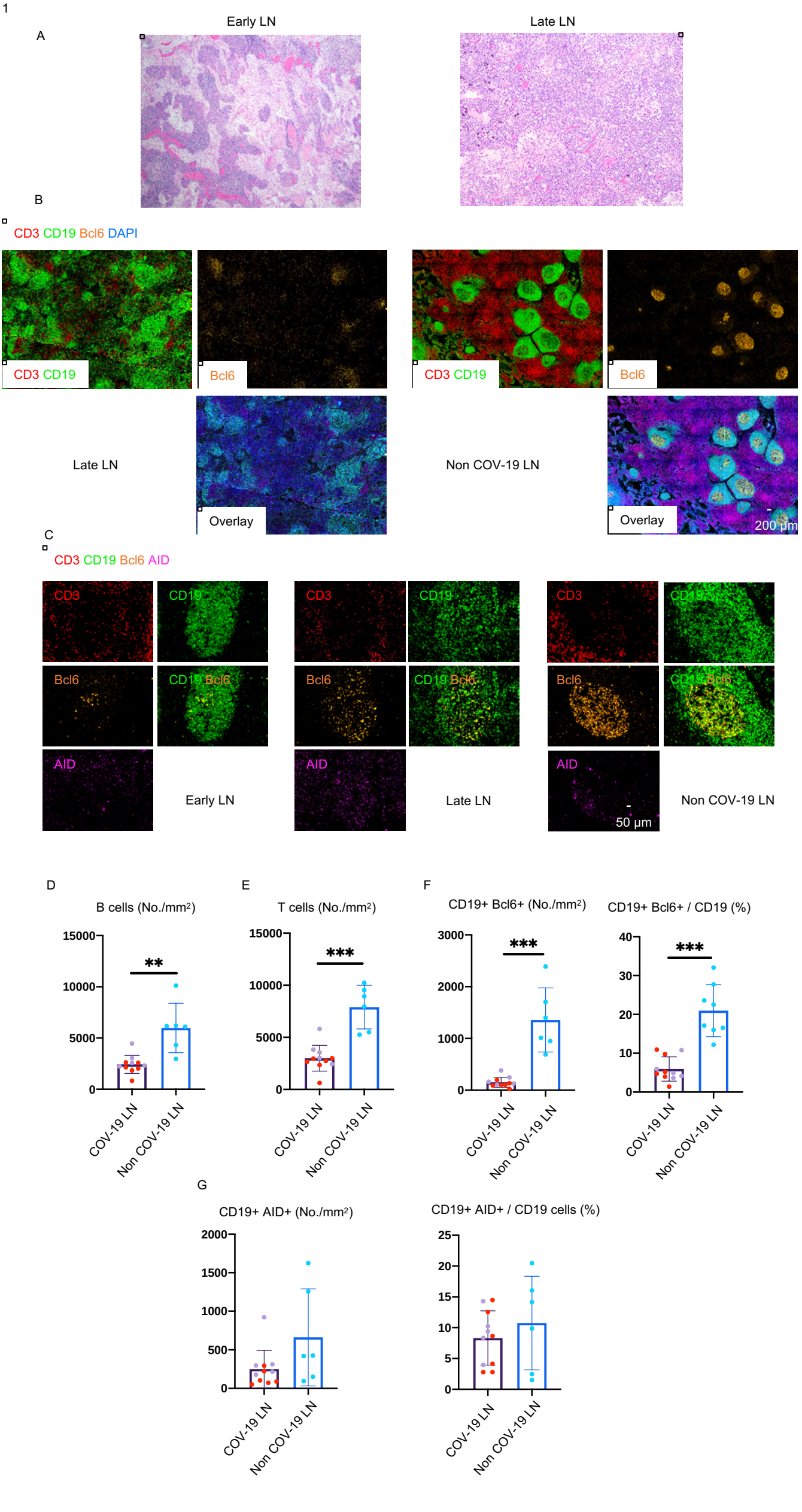
A
Early LN
Late LN
B
CD3 CD19 Bcl6 DAPI
CD3 CD19
Bcl6
Overlay
Late LN
Non COV-19 LN
200 µm
C
CD3 CD19 Bcl6 AID
CD3
CD19
Bcl6
CD19 Bcl6
AID
Early LN
Late LN
Non COV-19 LN
50 µm
D
B cells (No./mm²)
E
T cells (No./mm²)
F
CD19+ Bcl6+ (No./mm²)
CD19+ Bcl6+ / CD19 (%)
COV-19 LN
Non COV-19 LN
G
CD19+ AID+ (No./mm²)
CD19+ AID+ / CD19 cells (%)

Figure 2

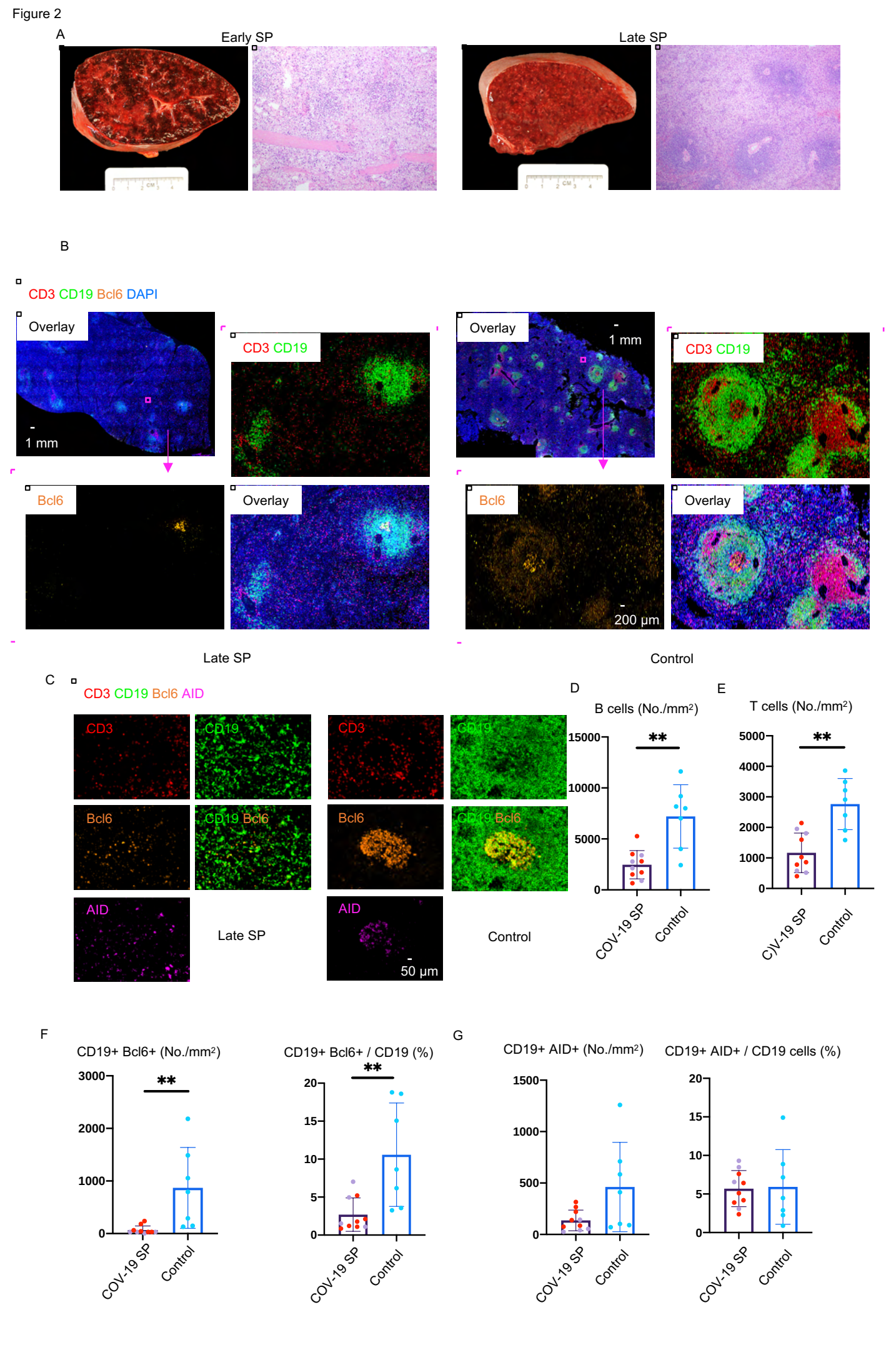
A
Early SP
Late SP
B
CD3 CD19 Bcl6 DAPI
Overlay
1 mm
CD3 CD19
Bcl6
Overlay
200 µm
Late SP
Control
C
CD3 CD19 Bcl6 AID
CD3
CD19
Bcl6
CD19 Bcl6
AID
50 µm
Late SP
Control
D
B cells (No./mm²)
15000
10000
5000
0
**
COV-19 SP
Control
E
T cells (No./mm²)
5000
4000
3000
2000
1000
0
**
COV-19 SP
Control
F
CD19+ Bcl6+ (No./mm²)
3000
2000
1000
0
**
COV-19 SP
Control
CD19+ Bcl6+ / CD19 (%)
20
15
10
5
0
**
COV-19 SP
Control
G
CD19+ AID+ (No./mm²)
1500
1000
500
0
COV-19 SP
Control
CD19+ AID+ / CD19 cells (%)
20
15
10
5
0
COV-19 SP
Control

Figure 3

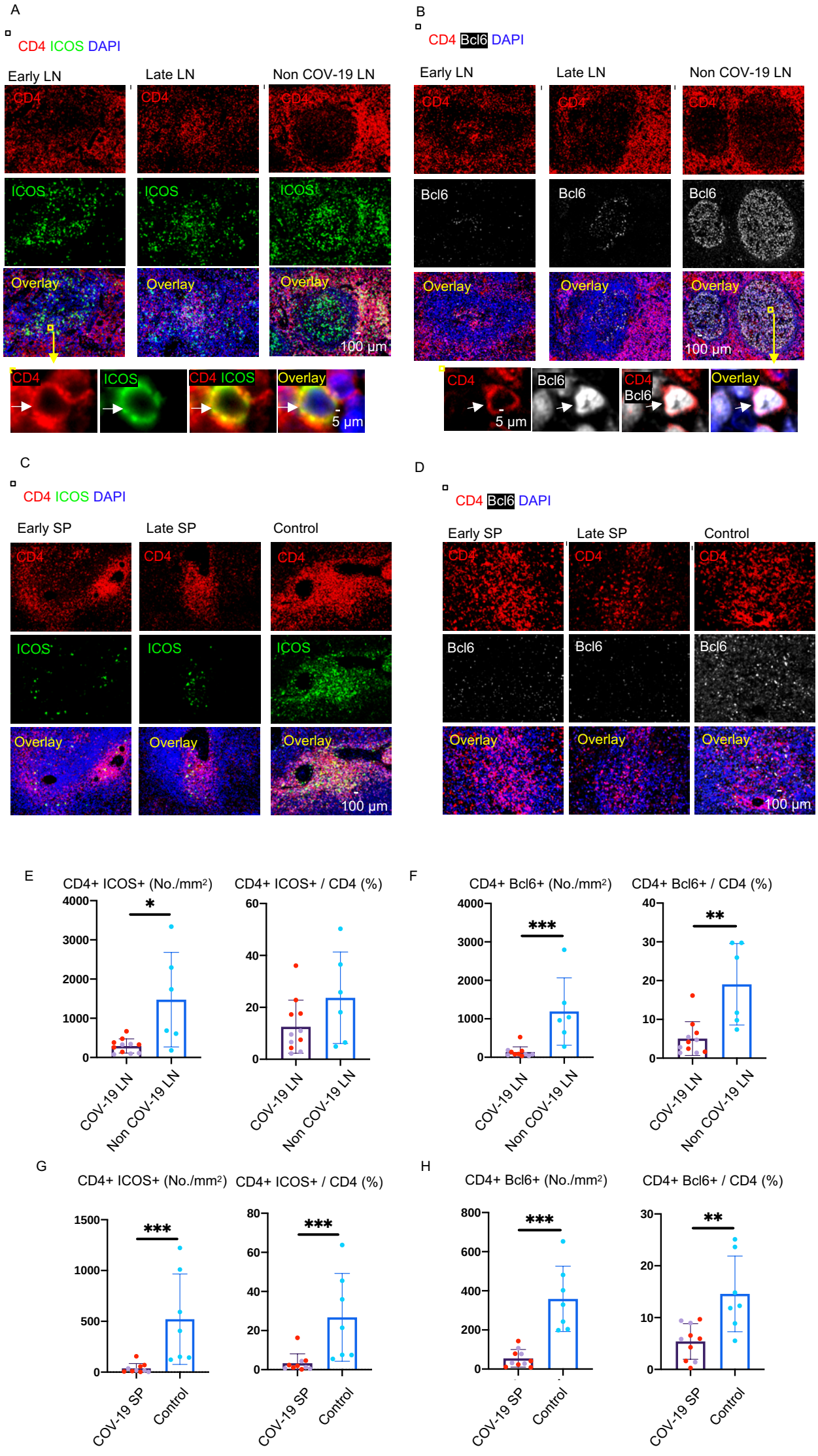
A
CD4 ICOS DAPI
Early LN
Late LN
Non COV-19 LN
CD4
ICOS
Overlay
100 μm
5 μm
B
CD4 Bcl6 DAPI
Bcl6
C
CD4 ICOS DAPI
Early SP
Late SP
Control
D
CD4 Bcl6 DAPI
E
CD4+ ICOS+ (No./mm²)
CD4+ ICOS+ / CD4 (%)
COV-19 LN
Non COV-19 LN
F
CD4+ Bcl6+ (No./mm²)
CD4+ Bcl6+ / CD4 (%)
G
COV-19 SP
Control
H

Figure 4

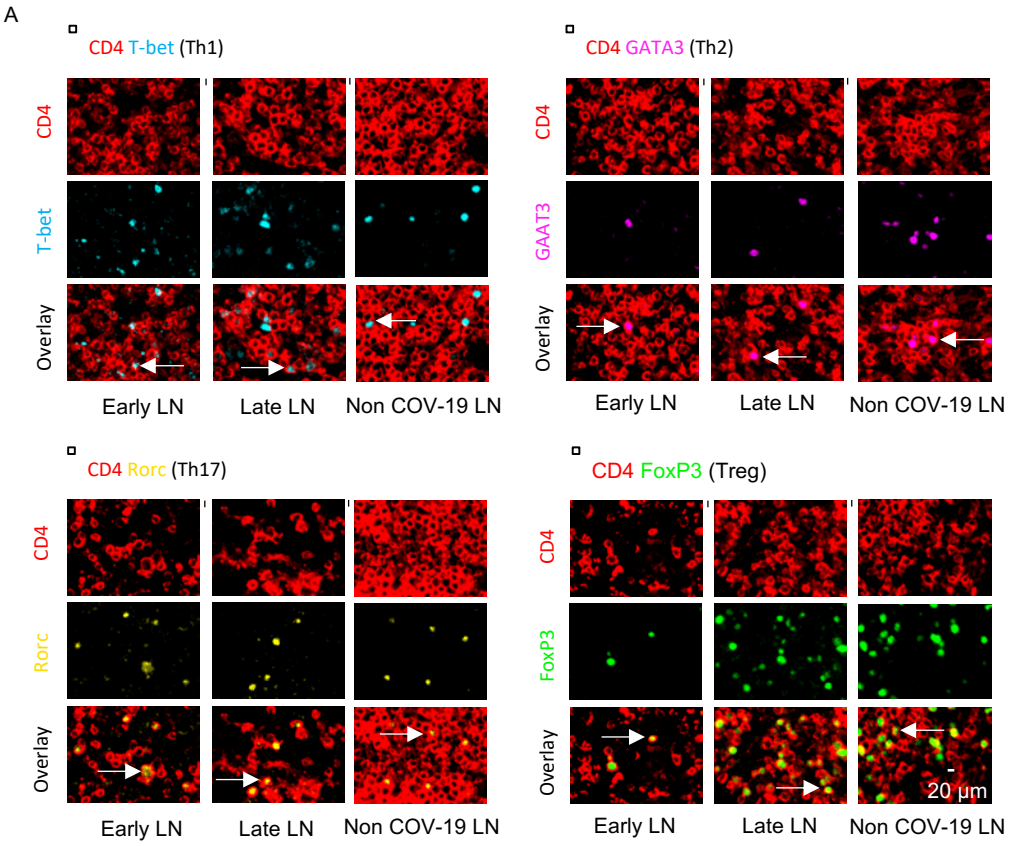
A
CD4 T-bet (Th1)
CD4
T-bet
Overlay
Early LN
Late LN
Non COV-19 LN
CD4 GATA3 (Th2)
CD4
GAAT3
Overlay
Early LN
Late LN
Non COV-19 LN
CD4 Rorc (Th17)
CD4
Rorc
Overlay
Early LN
Late LN
Non COV-19 LN
CD4 FoxP3 (Treg)
CD4
FoxP3
Overlay
20 µm
Early LN
Late LN
Non COV-19 LN

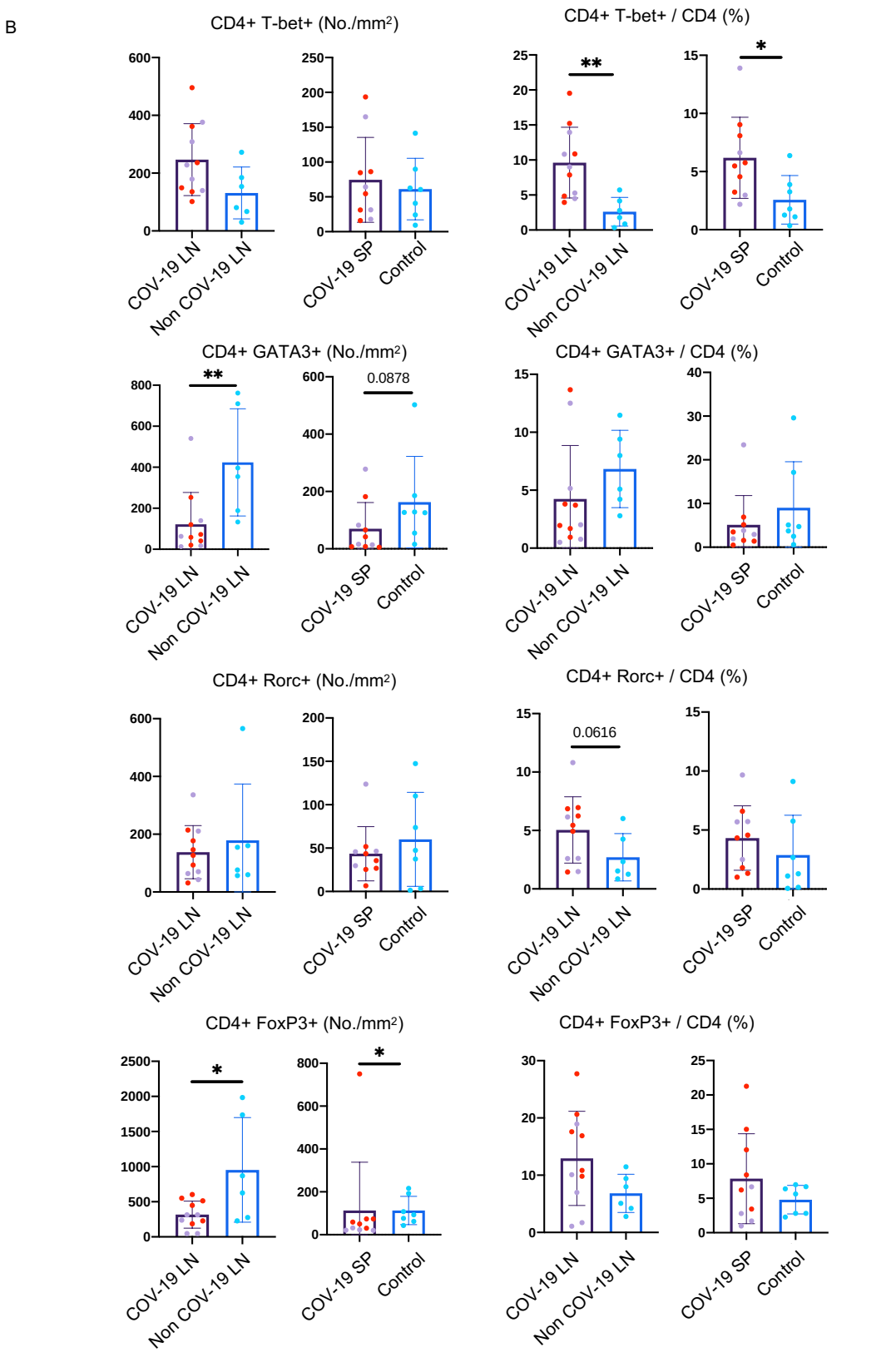
B
CD4+ T-bet+ (No./mm²)
COV-19 LN
Non COV-19 LN
COV-19 SP
Control
CD4+ T-bet+ / CD4 (%)
**
*
CD4+ GATA3+ (No./mm²)
**
0.0878
CD4+ GATA3+ / CD4 (%)
CD4+ Rorc+ (No./mm²)
CD4+ Rorc+ / CD4 (%)
0.0616
CD4+ FoxP3+ (No./mm²)
*
*
CD4+ FoxP3+ / CD4 (%)

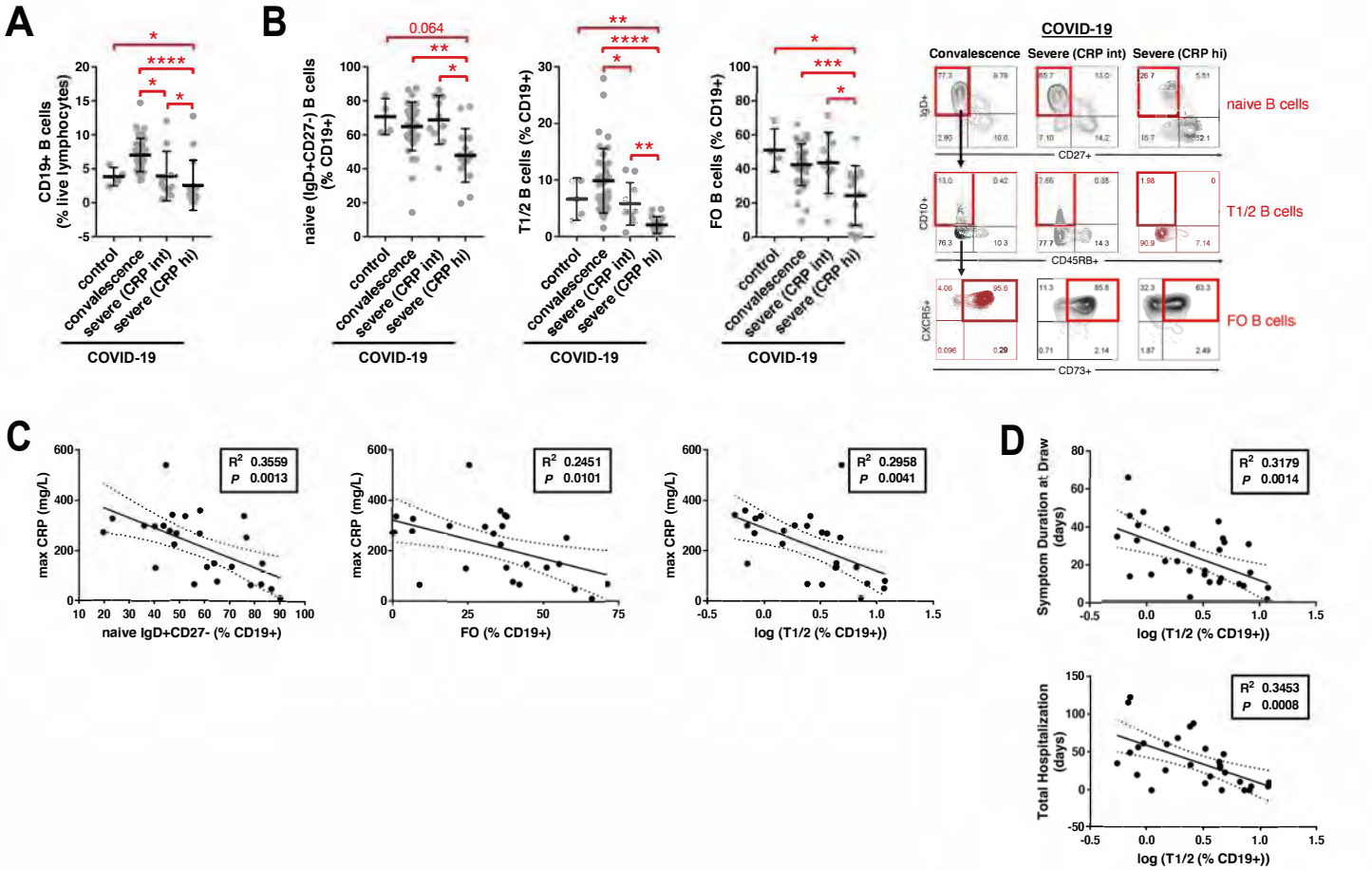
A
CD19+ B cells (% live lymphocytes)
control
convalescence
severe (CRP int)
severe (CRP hi)
COVID-19
B
naive (IgD+CD27-) B cells (% CD19+)
T1/2 B cells (% CD19+)
FO B cells (% CD19+)
0.064
COVID-19
COVID-19
Convalescence
Severe (CRP int)
Severe (CRP hi)
naive B cells
T1/2 B cells
FO B cells
IgD+
CD27+
CD10+
CD45RB+
CXCR5+
CD73+
C
max CRP (mg/L)
naive IgD+CD27- (% CD19+)
R2 0.3559
P 0.0013
FO (% CD19+)
R2 0.2451
P 0.0101
log (T1/2 (% CD19+))
R2 0.2958
P 0.0041
D
Symptom Duration at Draw (days)
log (T1/2 (% CD19+))
R2 0.3179
P 0.0014
Total Hospitalization (days)
log (T1/2 (% CD19+))
R2 0.3453
P 0.0008

Figure 6

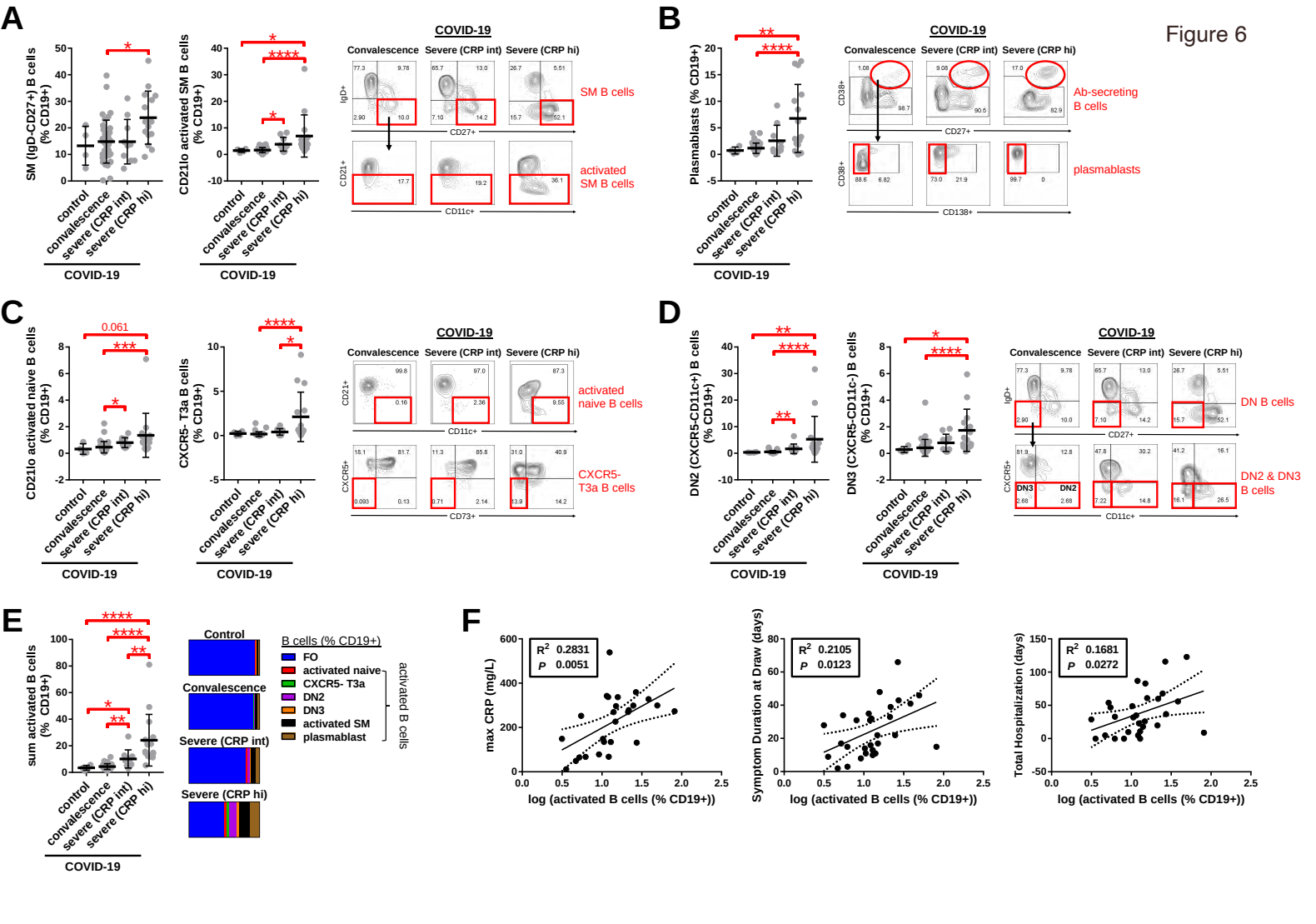
A
SM (IgD-CD27+) B cells (% CD19+)
CD21lo activated SM B cells (% CD19+)
control
convalescence
severe (CRP int)
severe (CRP hi)
COVID-19
COVID-19
Convalescence
Severe (CRP int)
Severe (CRP hi)
IgD+
CD27+
SM B cells
CD21+
CD11c+
activated SM B cells
B
Plasmablasts (% CD19+)
Ab-secreting B cells
CD38+
CD138+
plasmablasts
C
CD21lo activated naive B cells (% CD19+)
0.061
CXCR5- T3a B cells (% CD19+)
activated naive B cells
CXCR5+
CD73+
CXCR5- T3a B cells
D
DN2 (CXCR5-CD11c+) B cells (% CD19+)
DN3 (CXCR5-CD11c-) B cells (% CD19+)
DN B cells
DN2 & DN3 B cells
DN3
DN2
E
sum activated B cells (% CD19+)
Control
Convalescence
Severe (CRP int)
Severe (CRP hi)
B cells (% CD19+)
FO
activated naive
CXCR5- T3a
DN2
DN3
activated SM
plasmablast
activated B cells
F
max CRP (mg/L)
R2 0.2831
P 0.0051
log (activated B cells (% CD19+))
Symptom Duration at Draw (days)
R2 0.2105
P 0.0123
Total Hospitalization (days)
R2 0.1681
P 0.0272

Figure 7

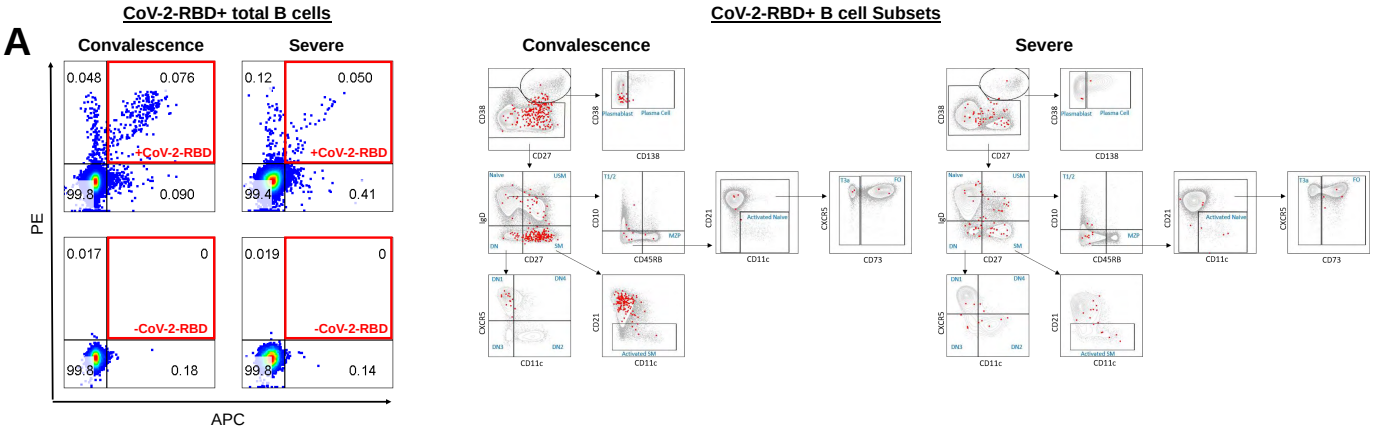
A
CoV-2-RBD+ total B cells
Convalescence
Severe
0.048
0.076
+CoV-2-RBD
99.8
0.090
0.12
0.050
+CoV-2-RBD
99.4
0.41
0.017
0
-CoV-2-RBD
99.8
0.18
0.019
0
-CoV-2-RBD
99.8
0.14
PE
APC
CoV-2-RBD+ B cell Subsets
Convalescence
Severe
CD38
CD27
CD138
IgD
CD10
CD45RB
CD21
CD11c
CXCR5
CD73

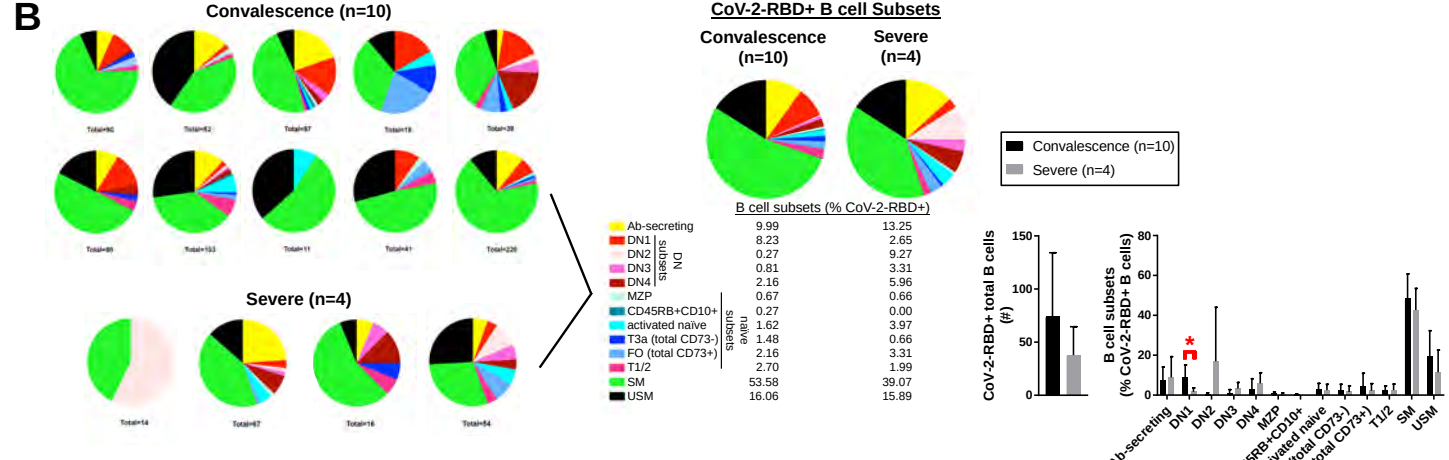
B
Convalescence (n=10)
Severe (n=4)
CoV-2-RBD+ B cell Subsets
Convalescence (n=10)
Severe (n=4)
B cell subsets (% CoV-2-RBD+)
Ab-secreting 9.99 13.25
DN1 8.23 2.65
DN2 0.27 9.27
DN3 0.81 3.31
DN4 2.16 5.96
MZP 0.67 0.66
CD45RB+CD10+ 0.27 0.00
activated naïve 1.62 3.97
T3a (total CD73-) 1.48 0.66
FO (total CD73+) 2.16 3.31
T1/2 2.70 1.99
SM 53.58 39.07
USM 16.06 15.89
DN subsets
naïve subsets
Convalescence (n=10)
Severe (n=4)
CoV-2-RBD+ total B cells (#)
B cell subsets (% CoV-2-RBD+ B cells)
Ab-secreting
DN1
DN2
DN3
DN4
MZP
CD45RB+CD10+
activated naïve
T3a (total CD73-)
FO (total CD73+)
T1/2
SM
USM